ARTICLE IN PRESS

International Journal of Mining Science and Technology xxx (xxxx) xxx



Contents lists available at ScienceDirect

International Journal of Mining Science and Technology

journal homepage: www.elsevier.com/locate/ijmst



Pull-out capacity and energy absorption of cable bolts under impact loading

Adel Mottahedi a,*, Naj Aziz a, Alex Remennikov a, Ali Mirzaghorbanali b

- ^a School of Civil, Mining, and Environmental Engineering, University of Wollongong, NSW 2522, Australia
- ^b School of Civil Engineering and Surveying, University of Southern Queensland, QLD 4350, Australia

ARTICLE INFO

Article history: Received 31 July 2025 Received in revised form 28 September 2025 Accepted 9 October 2025 Available online xxxx

Keywords:
Rock reinforcement
Cable bolt
Impact loading
Pull-out testing
Mine seismicity
Rock burst

ABSTRACT

This study investigates the performance of high-strength cable bolts under impact loading conditions representative of rock bursts in underground environments. Although widely used, the dynamic behaviour of these cable bolts has received limited experimental attention, and their effectiveness in seismically active zones remains a subject of ongoing debate. To address this gap, a reverse pull-out test machine integrated with a drop hammer rig was employed. Tests were conducted on 70-t SUMO bulbed and non-bulbed cable bolts with encapsulation lengths of 300 and 450 mm, subjected to an impact energy of 14.52 kJ. Results indicate that non-bulbed cables, despite showing lower initial peak loads (average 218 vs. 328 kN for bulbed cables at 300 mm encapsulation), demonstrated superior energy absorption (average 11.26 vs. 8.75 kJ) and displacement capacity (average 48.40 vs. 36.25 mm). Increasing the encapsulation length for bulbed cables led to a reduction in initial peak load but improved displacement and energy absorption. The dominant failure mechanism was debonding at the cable-grout interface, characterised by frictional sliding and cable rotation. These findings provide new insights into the energy dissipation mechanisms of cables and support the development of more resilient ground support systems for dynamically active conditions.

© 2025 China University of Mining & Technology. Publishing services by Elsevier B.V. This is an open access article under the CC BY license (http://creativecommons.org/licenses/by/4.0/).

underground opening [6].

1. Introduction

In underground mining and tunnelling projects, the safety of working spaces is always a paramount concern. To address this concern, stranded steel tendons, known as cable bolts, have been effectively employed as a rock reinforcement tool [1]. A cable bolt is a flexible tendon consisting of several steel wires, wound into a strand, which is grouted into a borehole [2]. The length of cables typically ranges between 3 and 15 m, while the rock bolt's length would generally be less than 3 m [3]. According to Fuller [4], the first application of cable bolt for rock reinforcement dates back to 1964 in South Africa, closely followed in Australia in the late 1960 s at the North Broken Hill, where 15 m long and 12.5 mm diameter cables were used. The principal function of tendons like cable bolts is to maintain and improve the strength of the rock mass, to prevent rock layer separation, and to control the postfailure deformation [5]. In this regard, cable bolts develop forces as the ground starts to move. The weight of the unstable rock block

 $\hbox{\it E-mail addresses: $am3887@uowmail.edu.au, adelmotahedi@gmail.com (A. Mottahedi).}$

carried out worldwide to investigate axial and shear capacities of cable bolts subjected to static loading mode, demonstrating the long-term ground settlements, during which no impact load is applied [1]. But tendons are also susceptible to impact loads, especially in dynamically active zones [8,9]. In the presence of seismic events (e.g., coal burst, rock burst, and large-scale blasting practices), high stress loading due to impact loading can also result in steel yielding, anchorage loosening, and maybe tendon complete failure [10]. Depending on the seismic event scale, the velocity of

ejected rock pieces may vary between 3 and 10 m/s, and the corresponding energy levels may vary from 10 to 50 kJ/m^2 [11,12], resulting in severe damage to underground openings as shown in Fig. 1. Thus, from a safety point of view, it is also necessary to

examine the performance of tendons under seismic loading.

close to the excavation boundary is conveyed to the firm rock strata beyond the unstable region in the roof and sidewalls of the

Since cable bolts play a pivotal role in resisting both axial load

due to the dead weight of the rock mass and shear load due to slip-

page along discontinuities [2,7], it is necessary to assess their per-

formance by subjecting them to both axial and shear loading

modes. Based on the available literature, various studies have been

https://doi.org/10.1016/j.ijmst.2025.10.013

2095-2686/© 2025 China University of Mining & Technology. Publishing services by Elsevier B.V. This is an open access article under the CC BY license (http://creativecommons.org/licenses/by/4.0/).

Please cite this article as: A. Mottahedi, N. Aziz, A. Remennikov et al., Pull-out capacity and energy absorption of cable bolts under impact loading, International Journal of Mining Science and Technology, https://doi.org/10.1016/j.ijmst.2025.10.013

^{*} Corresponding author.

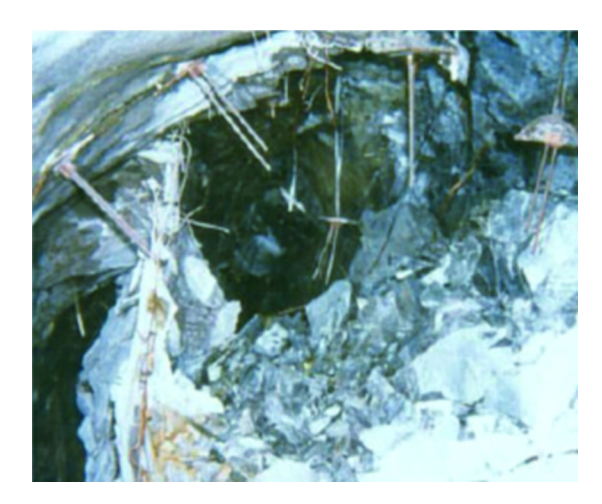


Fig. 1. An example of damage caused by a seismic event in an underground excavation [14].

To control the rock behaviour and cope with seismic loading, the tendon must be able to absorb the impact energy and accommodate the large rock displacement after the rock failure [11,13].

According to the literature, dynamic performance of rock bolts and cable bolts mainly assessed by using the following 2 methods [15]: direct impact (DI) method and momentum transfer (MT) method.

In the direct impact method, which can be utilised for both laboratory and in-situ tests, the impact energy is applied by a mass that freely falls onto the test sample. In the momentum transfer method, the test assembly, consisting of the mass and the test sample, free-falls at the beginning of the test until the movement of the assembly is stopped by a stopper, and the momentum of the mass is transferred to the test sample [9,16].

Dynamic testing of tendons began in North America, where Yan [17] tested small-diameter steel bolts. Since then, numerous studies have investigated the behaviour of energy-absorbing bolts under dynamic loading. Ansell [18] developed and tested a new energy-absorbing bolt, which yielded effectively under dynamic loads while maintaining structural integrity. Li [19] introduced the D-bolt as a solution for high-stress rock masses, showing elongation of 14%-20% and energy absorption of 47 kJ/m. Li and Doucet [20] tested D-bolts under dynamic loading, demonstrating high energy absorption (up to 60 kJ) and reliable performance due to their multi-anchor design. Knox and Berghorst [21] investigated the residual dynamic capacity of axially elongated energyabsorbing bolts, showing that while total energy absorption remains constant, prior strain reduces residual capacity. Crompton and Knox [22] extended this by examining the influence of bolt diameter, concluding that larger diameters improve elongation capacity, aiding restoration decisions. Darlington et al. [23] compared laboratory and in-situ dynamic testing of MDX bolts, finding consistent performance with minor variations due to installation methods. These studies have contributed to the development of safer, more resilient ground support systems.

More recently, innovations in cable bolt technology, such as dynamic yielding cables (e.g., Normet Dynamic Yielding Cables), have introduced advanced mechanisms for controlled deformation and energy dissipation. Such systems reflect a growing international trend toward yieldable support systems tailored for burst-prone environments. However, as shown in Table 1, most existing studies focus on low-strength cable bolts and there remains a lack of experimental data on the dynamic performance of high-strength

cables. Therefore, the current study, by undertaking further research on dynamic performance of high-strength cable bolts can complement current international efforts focused on yielding support systems and helps clarify the performance of high-strength cable bolts within the evolving landscape of energy-absorbing ground support technologies for underground mining and tunnelling.

In the case of high-strength cables, according to Table 1, Anzanpour et al. [25] carried out impact testing of an MW9 cable bolt. They apply 14.7 kJ of input energy, generated by dropping a 592kg mass from a height of 2.5 m onto the test specimen. This study explored that the required normalised energy (kJ/mm) for pulling the cable out of the host medium in the impact test was around 30% lower than that in the static test. Since the impact load was applied in a fraction of time, it was reported that the elimination of the effect of friction is the reason why the required pull-out load in the impact test was less. Later on, in the study conducted by Anzanpour et al. [26], the influence of cable bolt geometry was investigated through six impact tests on 63 t SUMO non-bulbed and bulbed cable bolts. To assess the absorbed energy, the area under the impact load-displacement curves was calculated. According to the results, it was reported that bulbed cables are a more reliable reinforcement system in seismically active grounds as they can absorb more impact energy (avg. 10 kJ) than that of non-bulbed cables (avg. 8.53 kJ). However, the accuracy of these energy measurements is questionable, as the load was recorded using a load cell mounted on the drop hammer rather than directly on the cable bolt. For precise results, the load should be calculated using the axial load cell mounted on the cable bolt. Hence, further experimental work is required to validate the previous results and make a specific conclusion.

Despite the widespread use of cable bolts in underground support systems, the dynamic performance of high-strength tendons under impact loading remains insufficiently understood. As a result, their behaviour in seismically active zones is still a topic of debate. Earlier studies have predominantly focused on lowstrength tendons and static loading conditions, leaving a gap in knowledge regarding how high-strength cables behave under rapid, high-energy impacts. This lack of reliable data can adversely affect the development of resilient support systems tailored to dynamically active ground conditions. Thus, the aim and motivation of the present research is to provide new insights into the energy absorption, displacement capacity, and failure mechanisms of high-strength cable bolts by conducting laboratory impact tests using a reverse pull-out test machine integrated with a drop hammer rig. These findings can contribute to improving the design of energy-absorbing ground support systems, enhancing safety and productivity in underground mining and tunnelling operations.

The paper has been arranged as follows: In Section 2, the materials, methodology of research, and the test procedure are demonstrated. In Section 3, the test sample preparation process is described in detail. In Section 4, the obtained results are presented and discussed. Finally, Section 5 concludes our findings.

2. Research methodology

2.1. Materials

In this research, to conduct impact pull-out tests, 70 t SUMO cable bolts with two different profile geometry have been utilised as high-strength tendons. The cable bolts have been manufactured and supplied by Jennmar Australia. Table 2 presents the details of the cables provided by the manufacturer. Also, according to the

International Journal of Mining Science and Technology xxx (xxxx) xxx

Table 1The earlier studies carried out on the axial performance of cables utilized impact pull-out testing.

Ref.	Impact loading pro	perties		Tendon properties			
	Loading option	m (kg)	h (m)	E (kJ)	V ₀ (m/s)	Cable type	Profile
Ortlepp and Stacey [27]	DI	1048		19.90		18 mm cable	Non-bulbed
Villaescusa et al. [28]	MT	2000	1.85	36.30	6.00	15.2 mm cable	Non-bulbed
Player et al. [11]	MT	2030	1.80	35.80	6.00	15.2 mm cable	Non-bulbed
Anzanpour et al. [25]	DI	592	2.50	14.50	7.00	31 mm MW9	Non-bulbed
Anzanpour et al. [26]	DI	592	2.50	14.50	7.00	28 mm 63 t SUMO	Non-bulbed/Bulbed
Pytlik and Szot [29]	DI	7300	0.45	32.20	1.50	15.7 mm cable	Non-bulbed

Note: E=mgh; $V_0=\sqrt{2gh}$.

Table 2The technical specifications of 70 t Sumo cable bolts [30].

Cable bolt properties		Cable bolt profile configuration		
Туре	SUMO			
Strand diameter (mm)	31			
Number of wires	12			
Wire type	Smooth	Nonbulbed cable bolt		
Bulb diameter (mm)	36			
Typical UTL (kN)	705			
Typical yield load (kN)	640	The same of the sa		
Breaking load with B&W (kN)	640			
Elongation (%)	5–7	Bulbed cable bolt		

required test arrangement, the bulbed version of the cables contained a single bulb (ex-clip) 150 mm from one end.

2.2. Impact testing facilities

2.2.1. Reverse pull-out test machine

In the domain of pull-out testing of tendons, the application of the single embedment pull test (SEPT) method has increased since the late 1970 s [1]. However, it was shown that the SEPT method is not able to prevent cable bolt rotation during laboratory-based tests, which is an unrealistic event as cables cannot unscrew in real field conditions [31]. Bawden et al. [32] showed that the cable rotation can underestimate its pull-out capacity. Thus, to address this issue, a new approach called the laboratory short encapsulation pull test (LSEPT) was introduced by Clifford et al. [33]. In this method, the free length of the cable is encapsulated in the anchor tube, indicating a length of the cable that is far away from the excavation boundary. Meanwhile, the end of the cable is encapsulated inside the host medium, simulating the rock mass sliding from the cable [34]. Based on the LSEPT approach, Anzanpour et al. [25] proposed a new pull-out apparatus, called the reverse pull-out test machine (RPTM), at the University of Wollongong (UoW). Utilising this apparatus, the tendon is pulled out of the host medium based on a push-to-pull loading mechanism.

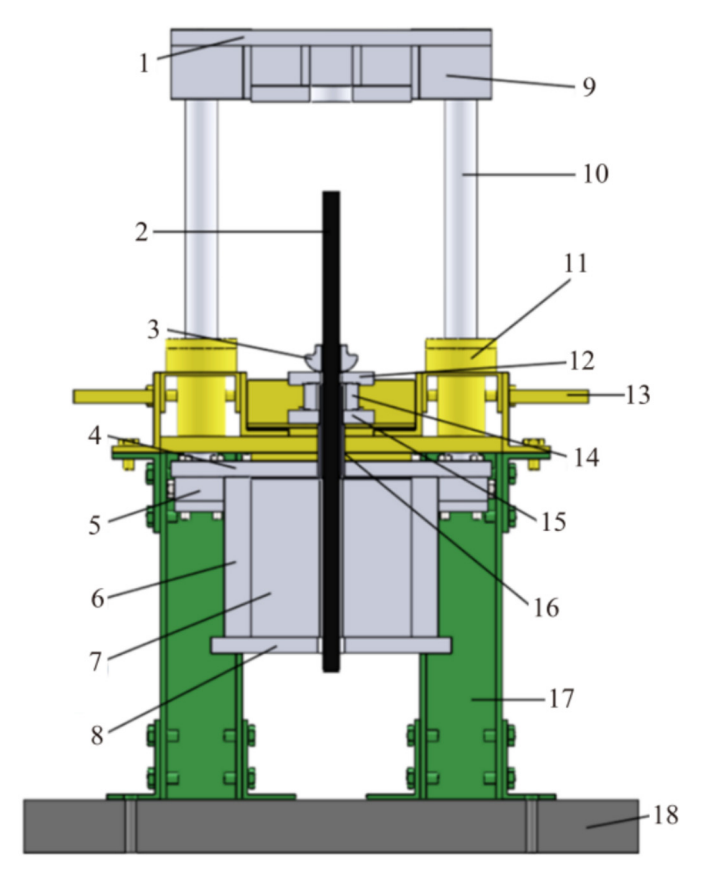
The RPTM and its main components are illustrated in Fig. 2. As shown, the load can be applied downward on the loading platform (1). Therefore, channels and plates are needed to reinforce the platform. The applied load is transferred to the confinement cage via four load-transferring shafts (10) and shaft holders (5). Four bearings (11) provide a smooth and frictionless track for the shafts, ensuring vertical movement. The confinement cage comprises a host medium (e.g., concrete cylinder) (7), top and bottom confinement plates (4&8), and a radial confinement cylinder (6). The cable (2) is held in place by the B&W (3) and the steel plate (12). A hollow load cell (14) is also located directly beneath the B&W plate to record the axial load. In addition, an anti-rotation confining tube

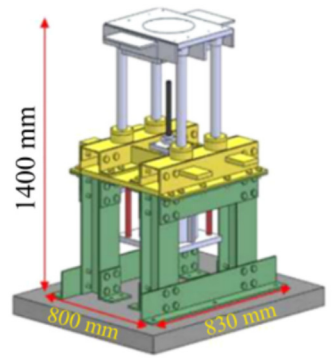
and plate (15&16) prevent the rotation of the cable during the test, limiting the movement of the anti-rotation tube only to the vertical direction [35].

As demonstrated in Fig. 3, once the load is applied, the moving parts of the rig are pushed down, including the loading platform, shafts, and the host medium. But the cable bolt is fixed in its initial position by a B&W leaning on a rigid frame. Thus, cable axial elongation or tensile failure, and grout-concrete and cable-grout interface failure are the permitted modes of failure [25]. It is noteworthy that the RPTM setup permits carrying out both static and impact loading tests, which is an advantage for a pull-out rig. Both cable bolts and rock bolts with different profile configurations can be tested. Besides, boreholes with different diameters and grout with various mechanical properties can be employed to assess their influence on the pull-out capacity of the tendon. For selecting the host medium diameter, it was found that Chen et al. [36] reported in their study that the load-bearing capacity of the cables increased with sample diameter up to 300 mm in confined conditions, and after this threshold, the capacity was approximately stable. Therefore, in the RPTM setup, cylindrical concrete samples of 300 mm diameter and 450 mm in height can be used as the host medium. This indicates that the influence of host medium strength and embedment length (up to 450 mm) can also be investigated using this rig [35].

2.2.2. Drop hammer rig

The drop-weight impact testing machine called drop hammer rig, designed based on the drop weight principle, is located in the Hi-Bay laboratory of the Faculty of Engineering and Information Sciences at the UoW. This rig has been built on a concrete foundation of $5.0 \, \text{m} \times 3.0 \, \text{m} \times 2.5 \, \text{m}$. The height of the rig is $6 \, \text{m}$, and the $592 \, \text{kg}$ free-fall hammer can be dropped from a maximum height of $4 \, \text{m}$ which is equivalent to the drop velocity of up to $9 \, \text{m/s}$ and $23 \, \text{kJ}$ of input potential energy [37]. The structure of the drop hammer rig and its key components are shown in Fig. $4 \, \text{m}$. The movement of the hammer is based on sliding between two guided col-





- 1. Loading platform
- 2. Cable bolt
- 3. Barrel and wedge (B&W)
- 4. Top confinement plate
- 5. Shaft holders
- 6. Radial confinement cylinder
- 7. Concrete sample
- 8. Bottom confinement plate
- 9. Reinforcement plates
- 10. Load transferring shafts
- 11. Bearings
- 12. B&W plate
- 13. Lifting wings
- 14. Hollow load cell
- 15. Anti-rotation plate
- 16. Anti-rotation confining tube
- 17. Fixed rigid columns
- 18. Reinforced ground

Fig. 2. The details of the RPTM setup and its key components.

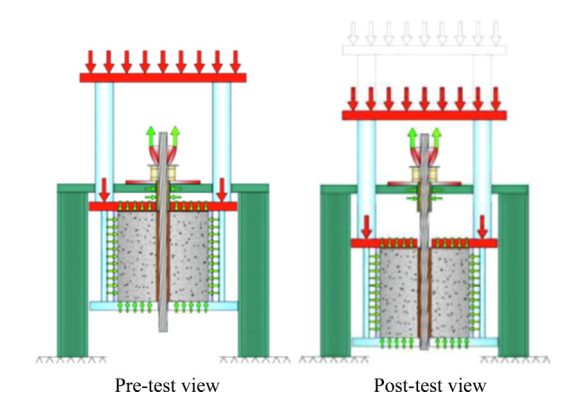


Fig. 3. The RPTM setup before and after the test, adopted from [35].

umns with rollers. To monitor and record the applied loads at the time of impact, a 1200 kN dynamic load cell (Interface Model 1200) is attached to the impactor.

2.3. Testing procedure

As it is schematically demonstrated in Fig. 5, to perform impact pull-out tests, first, the RPTM is placed under the drop hammer rig and anchored to the ground. Then, the drop hammer is elevated to the drop height of h. At this stage, the total input energy or the potential energy of the impactor ($E_{\rm im,p}$) can be determined as follows [17]:

$$E_{\rm im,p} = m_{\rm im}gh \tag{1}$$

where $m_{\rm im}$ is the drop hammer weight and g is the gravitational acceleration, 9.81 m/s². Besides, according to the energy equilibrium, the theoretical velocity $(V_{\rm im,0})$ of the impactor just before the strikes is equal to $(\sqrt{2gh})$ [9]. However, it was reported that during the hammer free fall, due to the friction of the guiding runner, the actual velocity of the impactor $(v_{\rm im,0})$ is 0.98 of its theoretical velocity [37]. Therefore, the kinetic energy of the impactor $(E_{\rm im,k})$ immediately prior to the strike onto the loading platform can be calculated by Eq. (2) [38]. Furthermore, the loss of energy due to the friction $(E_{\rm im,fr})$ is given as Eq. (3).

$$E_{im,k} = \frac{1}{2} m_{im} v_{im,0}^2 = \frac{1}{2} m_{im} [0.96(2gh)] \tag{2} \label{eq:energy}$$

$$E_{\text{im,fr}} = E_{\text{im,p}} - E_{\text{im,k}} = 0.04 m_{\text{im}} gh$$
 (3)

After the test initiation, the required data (e.g., impact load, displacement, etc.) are logged by using a data acquisition system that is able to collect 1000 data signals per second. It is a built-in chassis with coupled SCXI and SCI channels from National Instruments were used to acquire the experimental signals from the 24-channel strain gauge unit, the 4-channel digital voltage platform, and the eight-channel acceleration box [37]. Moreover, in the RPTM setup, the 900-kN capacity hollow axial load cell is installed on the cable bolt to record the applied impact load [35,38]. A noncontact ACUITY AR550-250 transducer, a high-speed laser sensor, is mounted on the apparatus to measure the displacement of the loading platform to a maximum range of 200 mm.

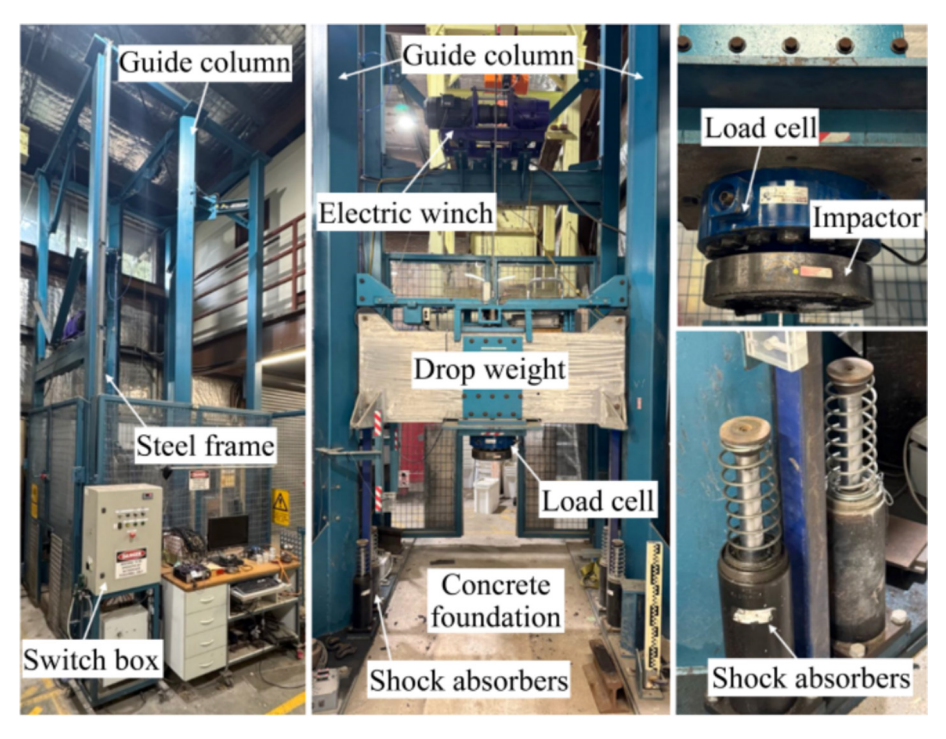


Fig. 4. A general view of the drop hammer rig test facility at the UoW.

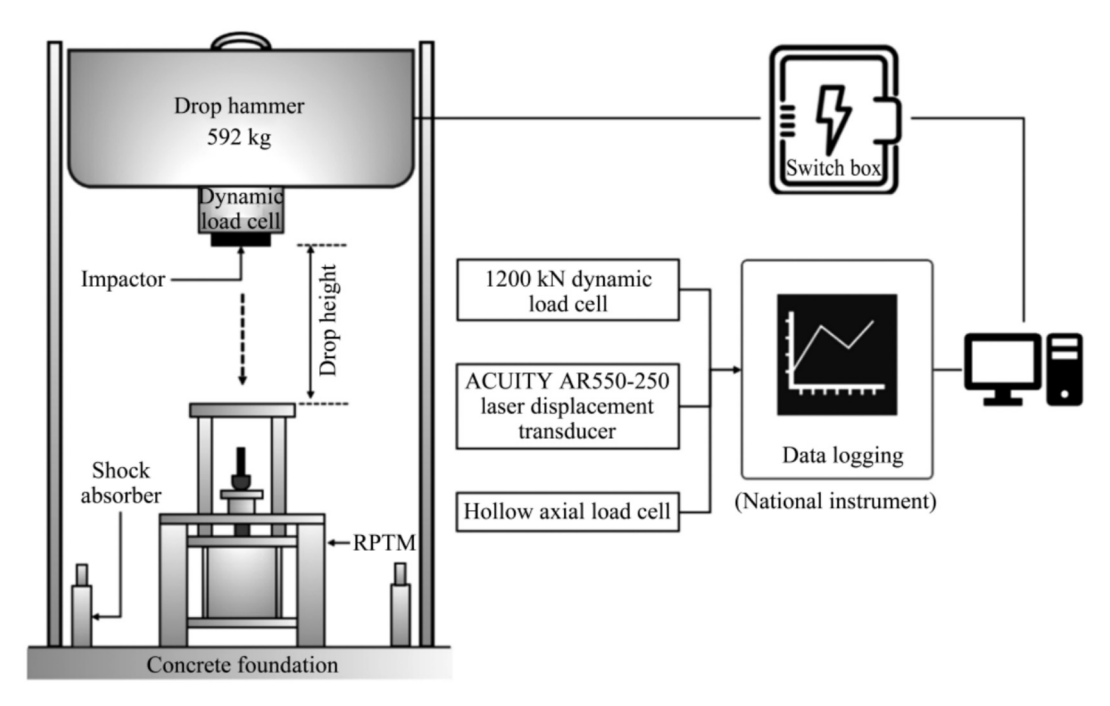


Fig. 5. A schematic view of the pull-out rig test arrangement under the drop hammer rig.

Table 3The experimental test plan for evaluating the dynamic pull-out capacity of the cable bolts.

Number of tests	Cable bolt type	LE (mm)	Input parameters						
			h (m)	$m_{\rm im}$ (kg)	$v_{im,0}$ (m/s)	$E_{\text{im,p}}$ (kJ)	$E_{\text{im,k}}$ (kJ)	E _{im,fr} (kJ)	
3	Bulbed	300	2.5	592	≈6.86	≈14.52	≈13.94	≈0.58	
3	Non-bulbed	300	2.5	592	≈6.86	≈14.52	≈13.94	≈0.58	
3	Bulbed	450	2.5	592	≈6.86	≈14.52	≈13.94	≈0.58	

A. Mottahedi, N. Aziz, A. Remennikov et al.

International Journal of Mining Science and Technology xxx (xxxx) xxx

2.4. Experimental test plan

The experimental test plan of this research is presented in Table 3. As shown, three tests are conducted per cable bolt type. It can be seen that the cable bolt profile geometry and length of encapsulation (LE) are the only variable parameters, and the rest of the influencing factors are kept constant for the test consistency. As a result, the effect of these two parameters on the pull-out capacity can be assessed by utilising the tests' outcomes. According to Eq. (1), and the configuration of the drop hammer rig, the drop height of 2.5 m can provide the potential energy of 14.52 kJ, which was designed to simulate moderate to severe rockburst conditions commonly encountered in deep mining environments. Rockburst events in underground mines can release energy ranging from 10 to 50 kJ/m², with ejection velocities between 3 and 10 m/s [11,12]. Therefore, the tested impact velocity of 6.86 m/s and

energy level of 14.52 kJ in this study correspond to dynamic loading scenarios observed in the field. It is also noteworthy that, based on Eq. (3), around 0.58 kN of the input energy is consumed by the friction.

3. Pull-out test assembly preparation

3.1. Casting concrete samples

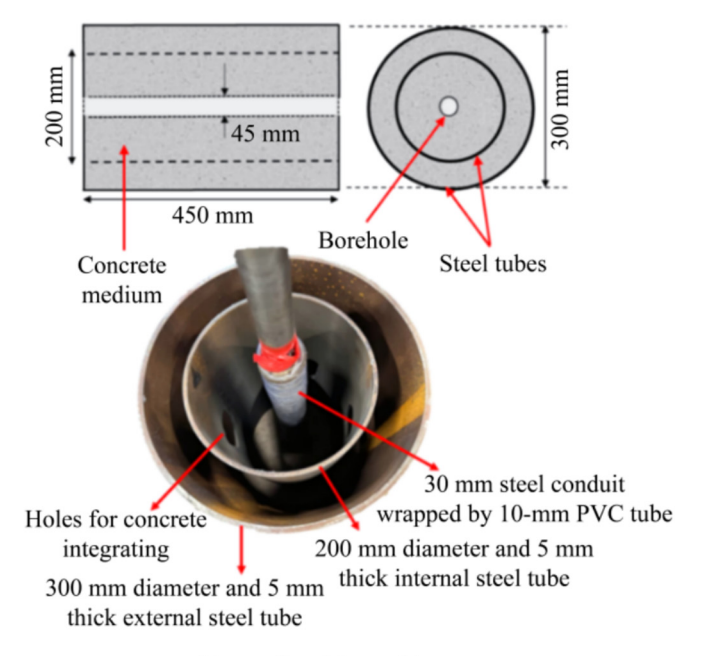
In Fig. 6, the details of the concrete sample preparation are illustrated. Over the last years, either cylindrical or cubic concrete samples, known as artificial rock specimens, have been mainly utilised for simulating the host medium conditions in pull-out testing of rock bolts and cable bolts. Possibly because it is mostly difficult to prepare rock samples of the required size for laboratory testing purposes [1]. Hence, in this research, according to the RPTM layout,



(a) Assembled molds for casting concrete samples



(c) Concrete pouring process



(b) Details of the molds



(d) Prepared concrete cylinders

Fig. 6. The assembled moulds for casting concrete samples (a), the details of the moulds (b), concrete pouring process (c), and the prepared concrete cylinders (d).

concrete samples with a diameter of 300 mm and a length of 450 mm can be used as a host medium for cable encapsulation. Meanwhile, to resemble the ground boundary condition, the constant radial stiffness (CRS) mode was employed as external confinement of the sample. This kind of external confinement simulates the restraint of surrounding soils or rock mass [31,39]. Therefore, when the test sample interacts with the confining medium, a CRS circumstance is formed, which replicates the changeable loading environment around the specimen [40].

Based on the earlier studies, it was shown that compared to the copper, Polyvinyl Chloride (PVC), and Aluminium tubes, the steel tubes were able to provide more effective confinement, resulting higher load transfer capacity (LTC) of the bolt during pull-out testing [41,42]. Thus, in this research, the samples were cast directly inside 300 mm diameter steel tubes with 5 mm of thickness. However, it has been found that, in either shear testing [38] or pull-out testing [25,35], the application of external confinement is not solely able to prevent sample cracking during pull-out testing. Generally, once the sample cracks, the test's outcome is highly likely to be unreliable and invalid. Hence, to address this issue, all concrete samples were also internally confined utilising 5 mm thick 200 mm diameter steel tubes. It was shown that the application of both internal and external confinements considerably improved the integrity of the test specimens during the tests by preventing the axial and lateral cracks development [26,35]. The positive influence of internal confinement in shear testing was also reported by Khaleghparast et al. [38]. It is noteworthy that, in the present study, the type, size, and thickness of the steel tubes were kept constant in all tests; therefore, a same level of radial stiffness was formed in all tests.

As shown in Fig. 6a, first, the external and internal steel tubes were cut and assembled in a specially prepared wood frame for the concrete pouring process. It is seen that the internal steel tubes had perforations to integrate poured concrete within and outside of the steel tubes (Fig. 6b). Furthermore, to simulate the central borehole for cable bolt encapsulation, 30 mm diameter cylindrical steel conduits were positioned at the centre of the steel tubes. To replicate the drill pattern and create borehole rifling, each conduit was wrapped with a 10 mm thick PVC tubes (hose). During the wrapping process, the PVC tube was intentionally stretched, resulting in a reduction of its nominal thickness and, consequently, its outer diameter. As a result, the final diameter of the wrapped conduit ranged between 42-45 mm, consistent with the required borehole diameter for installing 70 t SUMO cable bolts [30]. Borehole roughness provides a uniform bonding interface between the host medium and grout, reducing the grout-rock interface failure during the tests [43,44].

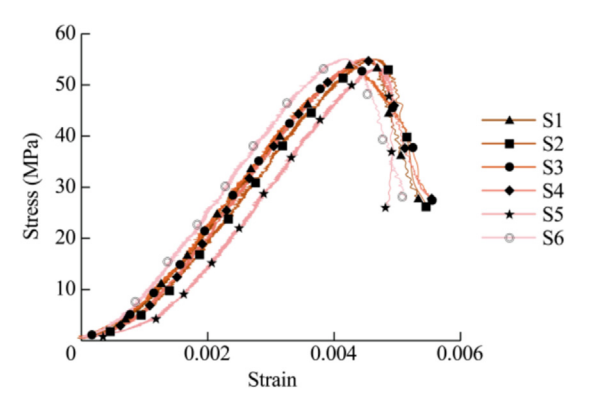


Fig. 7. The resulting stress-strain curves of the tested concrete samples.

Ultimately, as shown in Fig. 6c, concrete was poured inside the assembled moulds, and then the central steel conduits were hammered out of the cast sample after 24 h, when the initial hardening of the concrete was reached. As illustrated in Fig. 6d, a spiral groove remained on the surface of the boreholes when the PVC tubes were taken out. Next, the concrete specimens were covered with moisturised burlap fabrics for 28 d to age and reach their desired strength. Besides, for estimating the uniaxial compressive strength (UCS) of the concrete specimens, 100 mm diameter and 200 mm long cylindrical samples were prepared using the excess concrete and tested based on the established standards [45,46]. Accordingly, the strength test results are presented in Fig. 7. As shown, the average strength of the concrete was around 55 MPa.

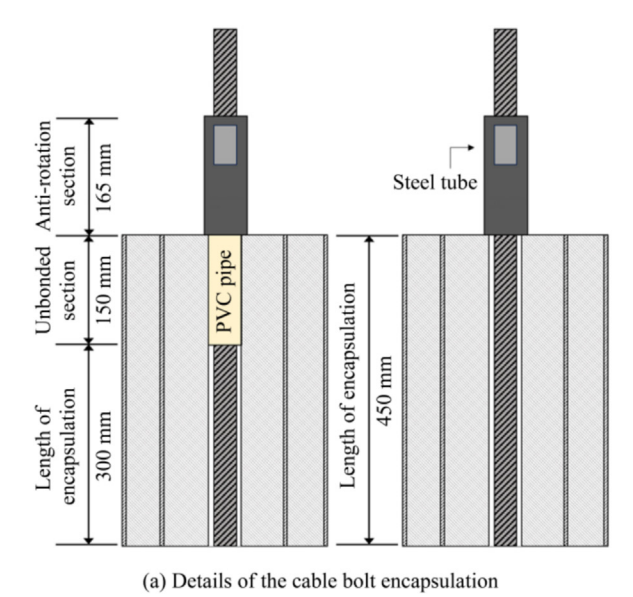
3.2. Cable bolt encapsulation

At this stage, 31 mm cable bolts need to be encapsulated inside the precast boreholes. For encapsulation purposes, the top-down 80 MPa grout (TD80) was used with a water-to-cement (w/c) ratio of 0.35 in all tests as recommended by the cable bolt's supplier. Regarding the length of encapsulation, based on the dimensions of the RPTM setup, the encapsulation length can vary between 300 to 450 mm. The earlier laboratory pull-out studies such as Hagan and Li [47] suggested that the length of encapsulation be at least equal to or longer than the lay length of the cable. As a result, the top 150 mm of the concrete cylinder was not bonded to the cable bolt for forming an encapsulation length of 300 mm.

As shown in Fig. 8 for the first six test samples, the 150 mm long unbonded sections were formed by encapsulating the cables in 40 mm diameter and 1.5 mm thick PVC pipes. Instead, for the last three test samples, as shown, to form 450 mm of LE, the cables were grouted in the whole length of the concrete cylinder. Meanwhile, to create the anti-rotation sections, 40 mm diameter and 4 mm thick steel tubes with flattened sides on opposite sides were installed and filled using the same grout. Then, the cementitious grout was poured into the boreholes, and the cables were installed inside the concrete sample. For preventing the grout leakage, the bottom ends of the boreholes were sealed. Besides, to increase the density and strength of the grout by eliminating the air pockets and packing the aggregate particles together, the cable bolts and concrete cylinders were vibrated during the grouting process. Ultimately, each prepared sample was left to be cured for 7 d before conducting the impact test. To determine the grout UCS, 50 mm cube samples were cast and tested according to the recommended standard (Fig. 9) [48].

3.3. Test specimen assembling

To prepare the test assembly for pull-out testing, the RPTM was assembled as shown in Fig. 10. In this regard, first, the test sample was placed on the bottom confining plate secured to the top confining plate by using four 25 mm internally threaded steel rods. It is noteworthy that to enhance the friction between the concrete samples and top/bottom confining plates, 3 mm thick rubber sheets were laid on/under the concrete sample. Next, the antirotation steel plates and bolts were placed to hold the antirotation tube firmly in position. The steel plates were rectangles with a half-circle cut on one side of each plate. Once the plates are placed around the tube, they are tightened to the side body of the rig by four bolts as shown. Thus, the plates act as a clamp around the tube to avoid rotations. Afterward, the hollow load cell and the B&W plate were installed, and the cable bolt was fixed by the B&W. In addition, a rubber matt was placed on top of the loading platform to prevent jarring load transfer when the drop weight impacted the platform. Finally, once the pull-out test specimen





(b) View of the prepared samples

Fig. 8. The details of the cable bolt encapsulation (a), and a view of the prepared samples (b).

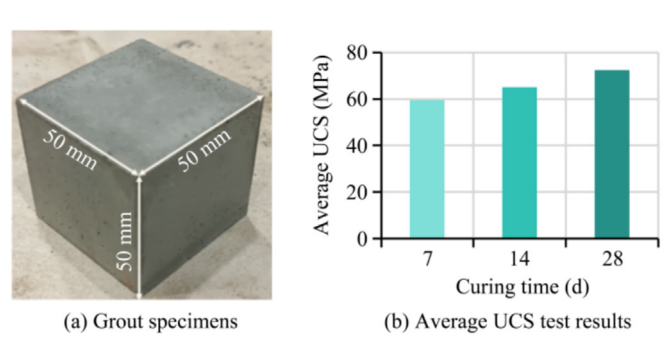


Fig. 9. The grout specimens (a), and the average UCS test results (b).

was fully assembled, it was lifted by the forklift and placed under the drop hammer rig for carrying out the impact test.

4. Results and discussions

4.1. Components of the impact load signal

The impact pull-out tests were conducted in accordance with the testing procedure and test plan explained in Sections 2.3 and 2.4. The time history curve of impact load along with displacement and pull-out load are shown in Fig. 11. As can be seen, the loading process involves different parts. St. Pierre et al. [12] reported that the loading signals, acquired during the impact tests, can be divided into three parts, including first impact, elastic rebounds, and system equilibrium. By using this classification, the curves can be divided into three parts as illustrated in Fig. 12.

As shown in Fig. 12, at the beginning of the first part, due to the conversion of the potential energy of the impactor into kinetic energy, a great amount of load is applied onto the loading platform. Since all the impact energy cannot be completely absorbed by the test specimen and the test rig, the remaining stored elastic energy is transferred back to the impactor in the form of kinetic energy, causing it to rebound [49]. Therefore, during the second part, the rebounds of the impactor form a series of bounces. In addition, the interval time between the bounces decreases progressively because the reduction in energy causes the impactor to rebound

less each time. Finally, the system returns to rest through a series of damped oscillations.

It is noteworthy that the first impact is the most important part in terms of loading amplitude and impact duration, producing permanent displacements. The obtained results also indicate that the subsequent bounces after the first impact were not able to change the permanent displacement significantly. This was also reported by the previous research [12,16,50]. The data obtained from the subsequent bounces can be considered artefacts, attributed to the stiffness of both the test apparatus and the bolt [16]. Hence, the major contributor to the cable bolt debonding and displacement is the first impact. In this regard, Fig. 13 shows the curves resulting from the initial loading to the time at which the load returns to zero.

4.2. Stages of the first impact load

As can be seen from Fig. 13, generally, the curves of the impact loads versus time can be divided into three stages. These three stages are explained and illustrated in Fig. 14, and described as follows:

- (1) Stage 1: Inertia effect stage: It is shown in Fig. 14 that once the impactor hits the loading platform at time zero, during 1.9 ms, the load significantly increases to the first peak load (FPL) of 1470 kN due to the inertial resistance of the stationary object (i.e., pullout rig) and then declines rapidly. It means that the load is transferred from the moving object (i.e., impactor) to the pull-out rig. Besides, as inertia is the immediate response of the impactor to the impact load, it does not represent the resistance of the sample against being pulled out.
- (2) Stage 2: Load-bearing stage: After Stage 1, the impactor and the test specimen begin to move downward together at Stage 2. Once the test specimen starts to displace, the load is being applied and transferred to the cable bolt at time 2.3 ms. Therefore, the impact load mainly works during Stage 2, which leads to the plastic deformation, like cable debonding at the cable-grout interface. The work done by the impact load at Stage 2 can also be shown by the time history curve of the pull-out loads recorded by the axial load cell installed on the cable bolt. According to the pull load-time curve, the load bearing of the cable bolt initiates at the beginning of Stage 2. Then, there is a pull-out load drop, meaning that deboning/failure takes place [12].

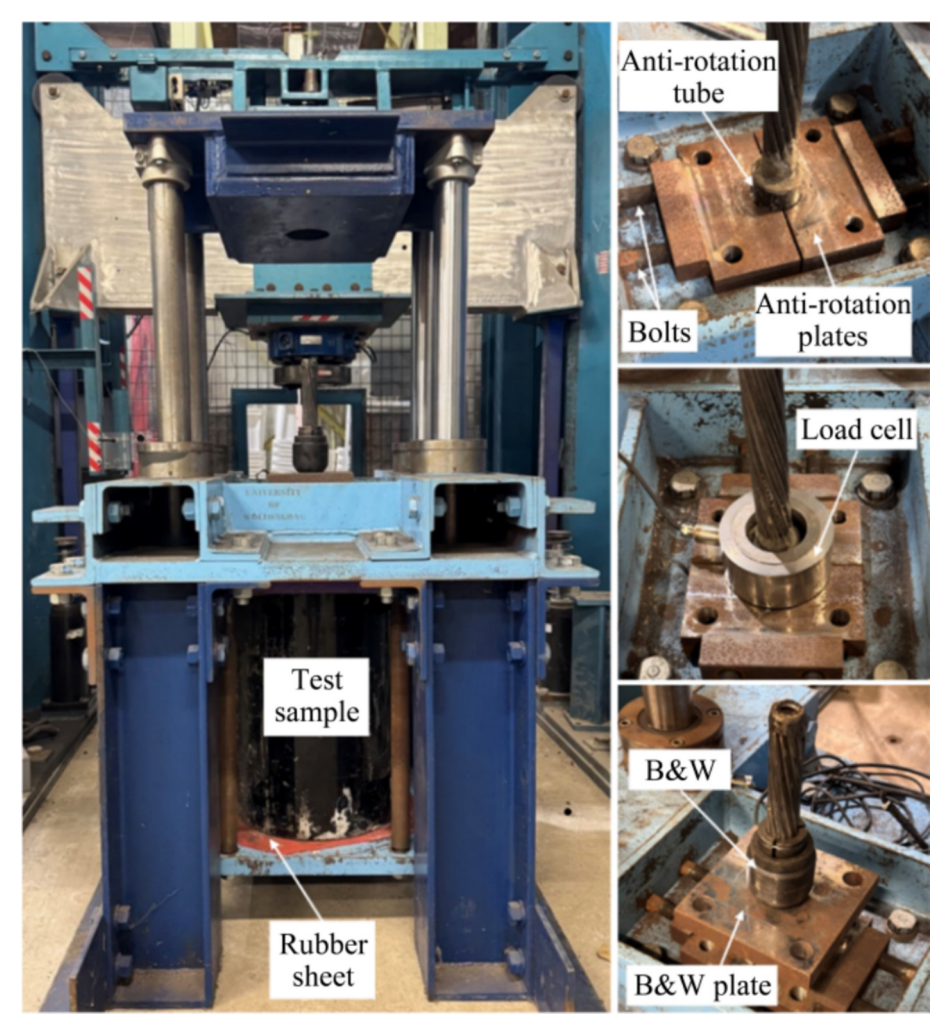


Fig. 10. A view of the assembled pull-out test specimen.

(3) Stage 3: Unloading stage: During Stage 2, as the recorded displacements show in Fig. 14, the displacement increases up to 44.80 mm at time 21.8 ms and then gradually reduces. Here, the displacement reduction indicates that the impactor starts to rebound upward due to the release of the stored elastic energy in the test specimen and the pull-out rig [12,16]. It means that the final stage starts with the decline of the load due to unloading. Thus, when the load ultimately reduces to zero at 41.9 ms, Stage 3 is finished, and the final displacement of 34.60 mm is obtained, which can be considered as the permanent displacement [16,20].

4.3. Comparison of the results

As shown in Fig. 13, there are fluctuations in the original pullout load recorded by the axial load cell during the impact test. The cause of this fluctuation is uncertain, but it could be linked to the response frequency of the strain-gauge sensors in the load cell [16]. Thus, in order to compare and interpret the obtained results meaningfully, first, the recorded pull-out load signals need to be smoothed. For this, the Gaussian smoothing, a method usually used for filtering time series was employed. An example of the original pull-out load signal versus the filtered signal is illustrated in Fig. 15. The filtered pull-out loads versus time are shown in Fig. 16. From the plotted curves, there are some variations among the results. The observed biases may be due to potential inconsistencies that take place during sample preparation, which need to be addressed in future research to obtain consistent outcomes. However, as observed, despite some variations in the plots, they generally follow a similar pattern, providing valuable insights into the similarities and differences between the cable types.

4.3.1. Pull-out behaviour profile

The characteristics of the load-displacement and load-time curves of the tested bulbed cable bolts are illustrated in Fig. 17a. According to the loading profiles of the tested bolts, the pull-out process can be divided into three main regions, including nonlinear elastic, elastoplastic, plastic, and unloading regions. It is seen that, during the non-linear elastic region, the bulbed cable starts to carry the load from point "A". Here, the loading path exhibits hardening behaviour, indicating that resistance to deformation increases as the load rises over time. The bond strength between the cable and grout, intensified by bulbing, plays an important role at this stage. However, as seen, after point "B", there is a "pop-in" behaviour in the load-displacement curve, characterizing with an abrupt displacement increase at a particular load [51].

Pop-in behaviours are generally interpreted as defects (e.g., micro-cracks, pores, interface between hard material and soft materials) that allow for plastic deformation. They indicate the transition from elastic deformation to plastic deformation. Then, the plastic region begins with the FPL and is followed by a considerable displacement rise as the load-bearing capacity reduces. Therefore, it can be said that debonding takes place at this stage.

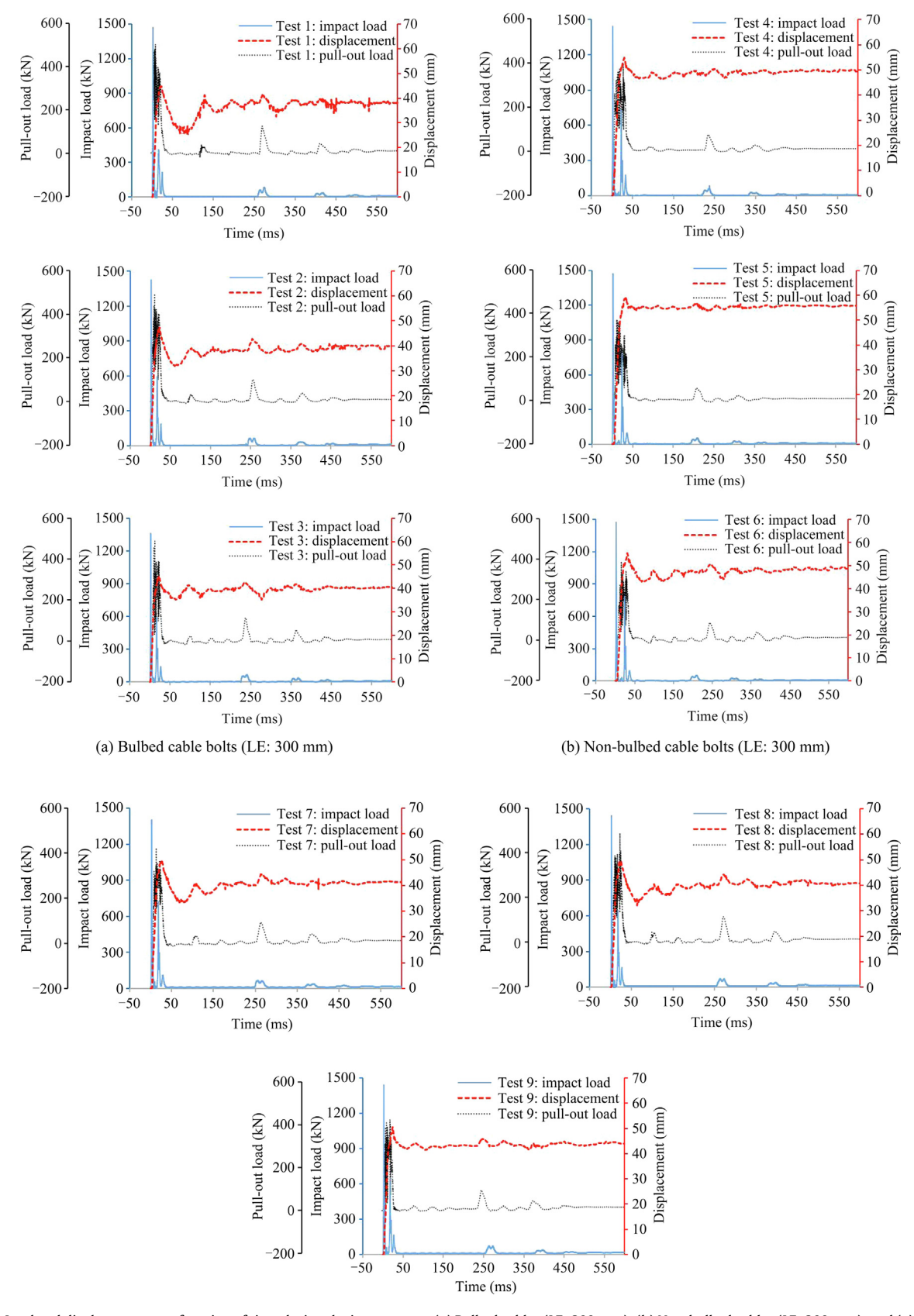


Fig. 11. The Load and displacement as a function of time during the impact tests: (a) Bulbed cables (LE: 300 mm); (b) Non-bulbed cables (LE: 300 mm); and (c) Bulbed cables (LE: 450 mm).

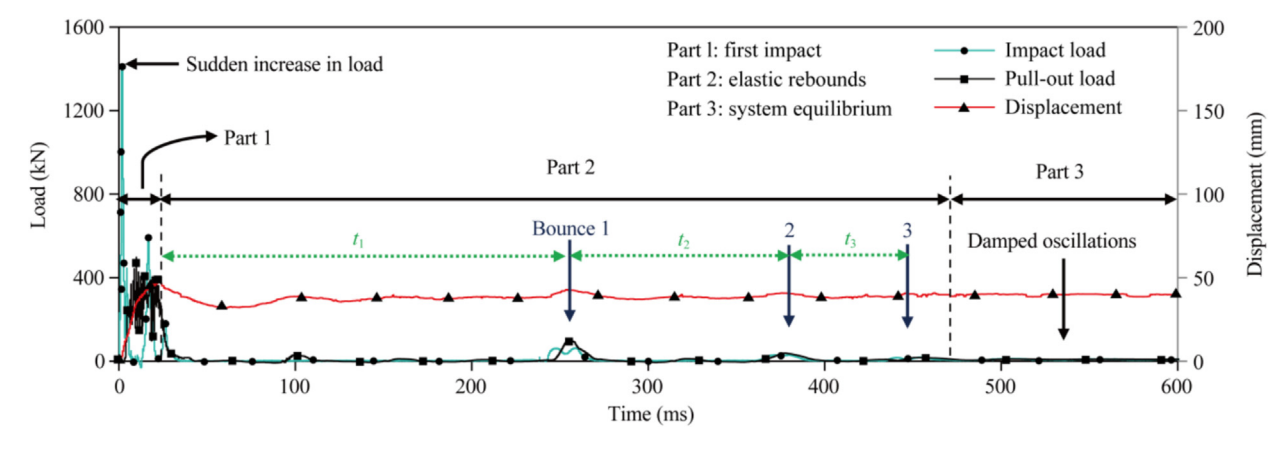


Fig. 12. The classification of the loading signal (Test 2).

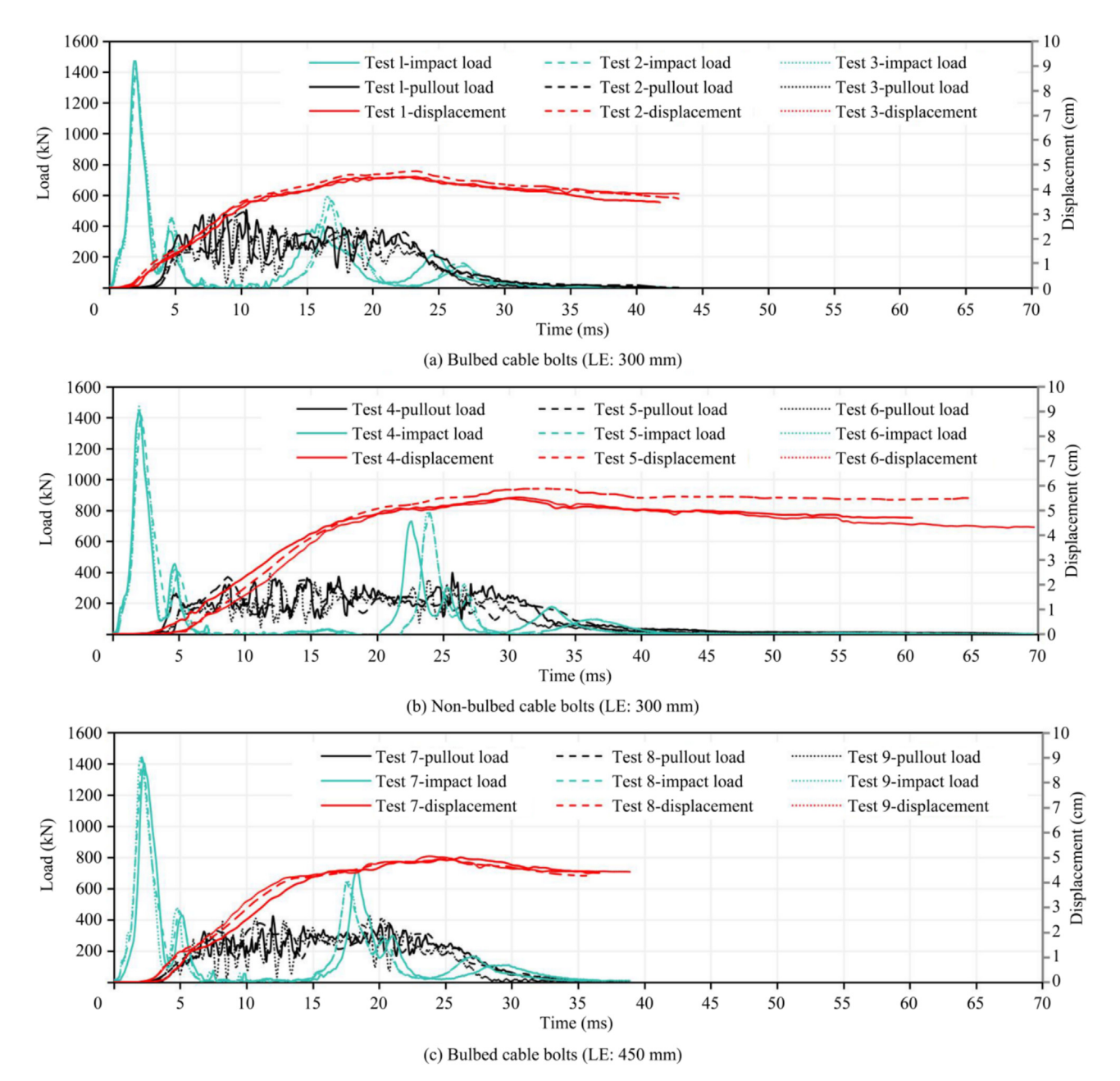


Fig. 13. The load and displacement as a function of time during the first impact.

A. Mottahedi, N. Aziz, A. Remennikov et al.

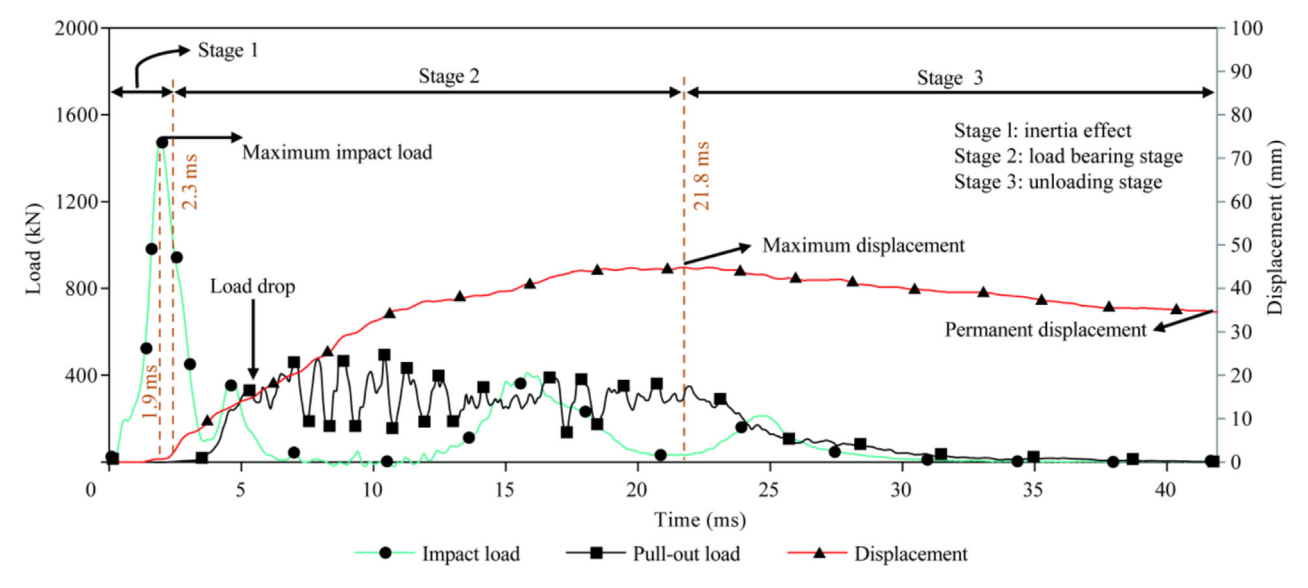


Fig. 14. The stages of the loading signal during the first impact (Test 1).

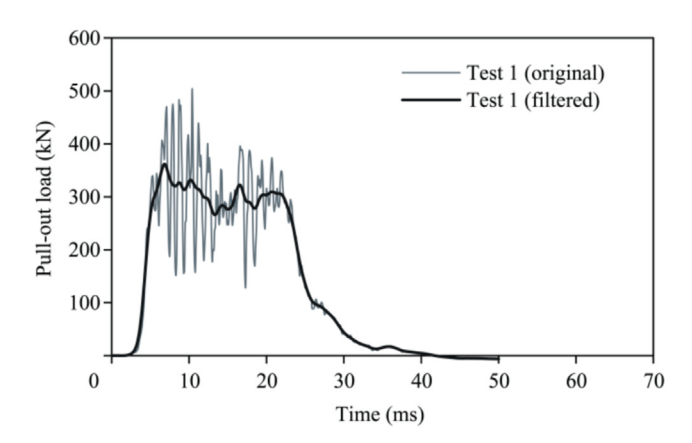


Fig. 15. The original pull-out load signal versus the filtered signal.

As can be seen, the maximum displacement is reached at point "D" where the impactor starts to rebound, and the unloading region commences. It is noteworthy that the duration from point "C" to "D" is defined as the impact duration (t_i) (Fig. 17b) [20]. During this stage, the elastic deformation is recovered, and when the load reduces to zero at point "E", the instrument-measured irreversible or plastic displacement ($d_{\rm p,i}$) is obtained. The plastic displacement might be the results of both cable bolt strand elongation and displacement.

Fig. 18 also shows the characteristics of the loading profile of the tested non-bulbed cable bolts. As illustrated in Fig. 18a, the load-displacement curve can be divided into four main regions similar to the bulbed cable bolts. However, in this case, the behaviour of the curve at the early stages is bilinear, characterising with an almost vertical part. This may be due to a delayed response from the laser displacement sensor. The transition from the elastic to the plastic region begins at point "B". Following the pop-in behaviour, the FPL is reached at point "C", marking the onset of the plastic stage. As can be seen, this stage involves meaningful deformation until the ultimate displacement is achieved at point "D". Subsequently, the unloading begins, and the pull-out load reduces to zero at point "E" where the permanent displacement is attained.

Comparing the load-displacement curves of bulbed and nonbulbed cable bolts shows that the load-bearing capacities of the bulbed cables were greater than that of non-bulbed ones. Besides, the information presented in Table 4 showed when LE was 300 mm, on average, the bulbed cable bolts required more FPL (about 328 kN) in comparison with the non-bulbed ones (approximately 218 kN). The presence of a bulb in cable bolts enhances mechanical interlocking, acting as a mechanical anchor. This configuration allows bulbed cable bolts to transfer higher loads before debonding under impact loading conditions. However, when evaluating displacement capacity, non-bulbed cable bolts demonstrate greater flexibility. Regardless of their lower load-bearing capacity, they accommodate larger displacements (48.40 mm) compared to bulbed cables (36.25 mm). This increased displacement suggests that non-bulbed cable bolts may be more suitable for dynamically active ground conditions, where greater deformation can contribute to more effective impact energy dissipation. As shown in Table 4, this behavior is further supported by the comparison of impact durations: non-bulbed cable bolts, on average, sustained the impact load for a longer period (approximately 28.50 ms), indicating a more prolonged energy absorption process.

As presented in Table 4 and Fig. 19, variations in LE influence the mechanical response of bulbed cable bolts under impact loading conditions. It was found that an increase in LE resulted in a reduction of the average FPL from 328 to 248 kN. Analysis of the load-displacement curves indicates that, within the plastic deformation region, cable bolts with longer LE showed increasing pullout loads, eventually reaching load levels comparable to those observed in bolts with an LE of 300 mm. This suggests that while the initial stiffness may differ, the ultimate load-bearing capacity converges across different LE configurations. Moreover, despite the decrease in FPL, the axial displacement capacity improved from 36.25 to 43.26 mm, indicating enhanced energy absorption capability during impact events. Furthermore, extending LE from 300 to 450 mm led to an increase in impact duration from 19.80 to 22.37 ms. This suggests that the cable bolt system was able to sustain the impact load over a longer time interval, thereby improving its ability to dissipate energy and reduce the severity of impactinduced damage.

Although variations in *LE* did not produce a significant change in the ultimate load-bearing capacity under impact loading conditions, previous studies have consistently reported that under static pull-out testing, the load-bearing capacity increases with *LE* [52,53]. This discrepancy highlights the influence of loading mode

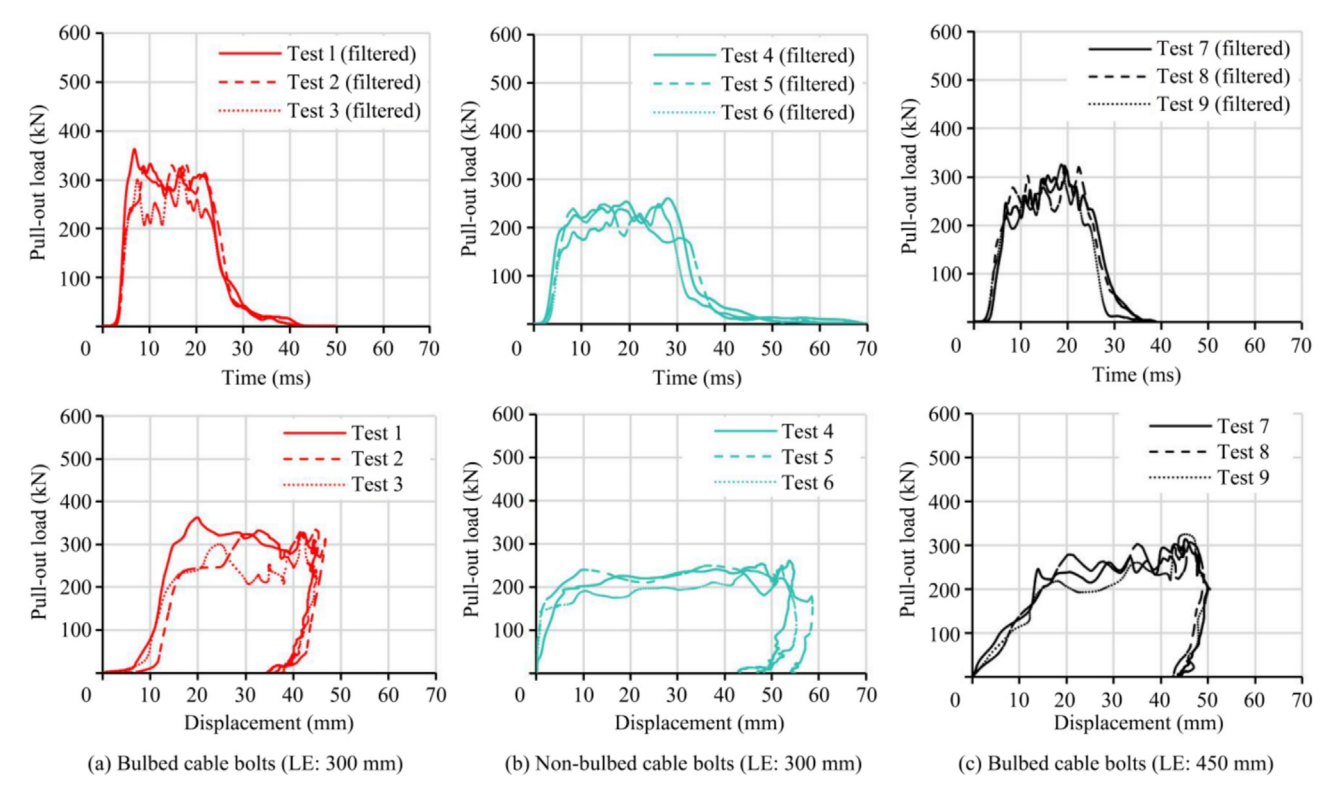


Fig. 16. The pull-out load-time and load-displacement curves.

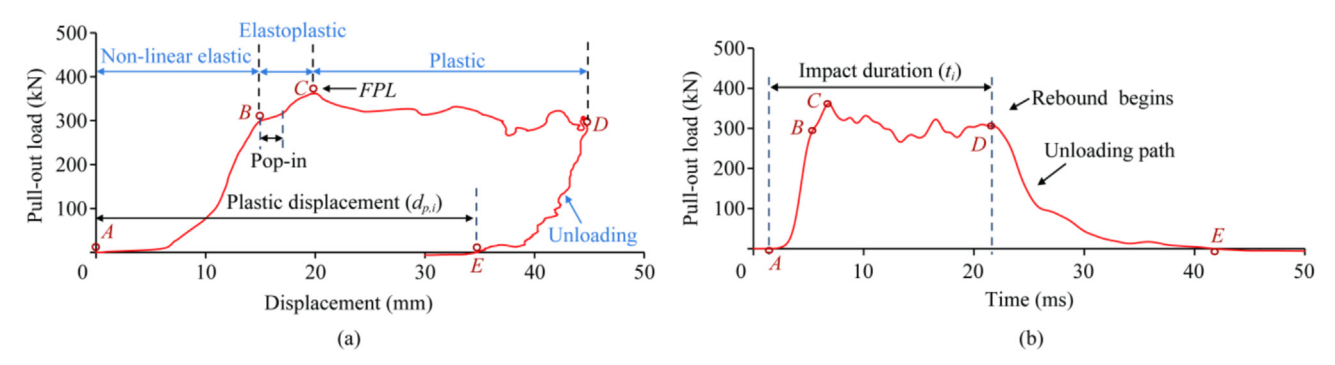


Fig. 17. The features of the load-displacement and load-time curves of the bulbed cable bolt (Test 1).

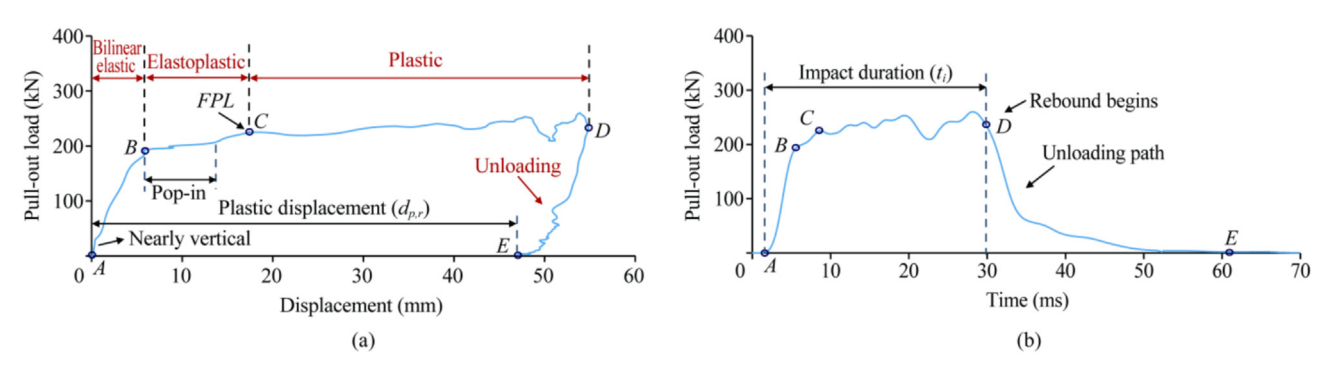


Fig. 18. The features of the load-displacement and load-time curves of the non-bulbed cable bolt (Test 4).

on the mechanical behaviour of cable bolts. Therefore, to draw a definitive conclusion regarding the role of LE in dynamic performance, further impact testing across a broader range of encapsulation lengths is necessary.

4.3.2. B&W response to the load

During the impact tests, none of the employed B&W units failed; however, as shown in Fig. 20, some inward movement of the wedge within the barrel was observed as the B&Ws were not

A. Mottahedi, N. Aziz, A. Remennikov et al.

Table 4The details of the pull-out load profiles.

Test No.	Bolt type	LE (mm)	FPL (kN)	Ave. FPL (kN)	$d_{p,i}$ (mm)	Ave. $d_{p,i}$ (mm)	t _i (ms)	Ave. t_i (ms)
1	Bulbed	300	361.82	328.31	34.60	36.25	19.50	19.80
2	Bulbed	300	324.10		36.07		19.20	
3	Bulbed	300	299.01		38.08		20.70	
4	Non-bulbed	300	224.98	217.91	46.98	48.40	26.70	28.53
5	Non-bulbed	300	238.65		54.98		31.10	
6	Non-bulbed	300	190.11		43.24		27.80	
7	Bulbed	450	245.11	248.21	43.74	43.26	22.60	22.37
8	Bulbed	450	281.63		41.86		22.30	
9	Bulbed	450	217.90		44.17		22.20	

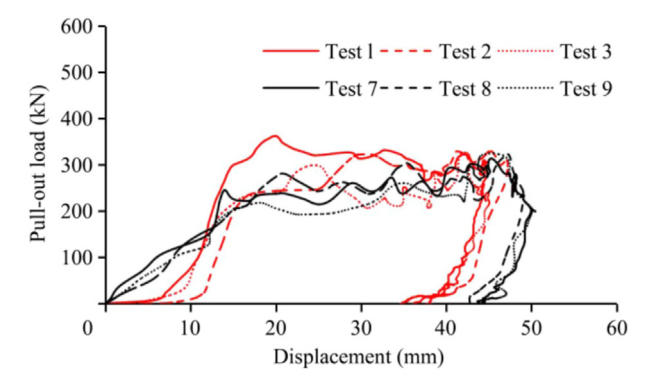


Fig. 19. Comparing the load-displacement curves of bulbed cable bolts with different LE.

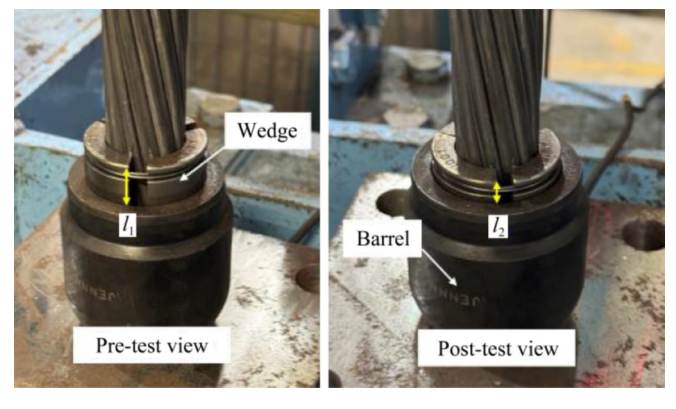


Fig. 20. An example of the status of B&W before and after the impact test.

fixed. As a result, the B&W displacement $(d_{\text{B\&W}})$ contributed to the instrument-measured plastic displacement $(d_{\text{p,i}})$. To quantify this contribution, the initial and final displacements of the B&W were measured before and after the tests. It is worth mentioning that,

due to the time constraints, LVDTs (Linear variable differential transformers) could not be used to record the real-time deformation of the B&W during the impact tests. According to the results presented in Table 5, after subtracting the B&W displacements from the instrument-measured plastic displacements, the final plastic displacements ($d'_{\rm p,f}$) of the cable bolts are achieved. By comparing the $d'_{\rm p,f}$ with the manually measured plastic displacements ($D_{\rm p,m}$), it can be seen that there is a displacement deviation ($\delta_{\rm d}$) ranging between 0 to 19%.

This discrepancy, reaching up to 19%, can be attributed to several factors. The instrument-measured displacement was recorded using a factory-calibrated laser displacement sensor. However, despite factory calibration, potential sources of error such as mounting misalignment, transient vibrations, and shock during high-speed impact loading may introduce noise into the readings and affect sensor stability, particularly at the moment of hammer strike. On the other hand, manual measurements were taken post-test using a tape measure and visual inspection, a method inherently prone to human error like subjective interpretation of deformation endpoints. These limitations, combined with the dynamic nature of the testing environment, contributed to the observed variation. For future studies, the use of high-speed video tracking is recommended to improve measurement reliability and cross-validation.

4.3.3. Pull-out mechanism

According to Hutchinson and Diederichs [2], there are some possible failure modes/mechanisms of a cable bolt reinforcement system, including cable's wire (strand) failure, debonding at cable-grout interface, and debonding at grout-rock interface. In this research, to determine the failure mode, the tested cylindrical specimens were cut open to produce bi-sectional views. Initially, longitudinal cuts were made using a diamond-blade concrete saw to guide crack propagation. Steel wedges were then inserted into these cuts, and a hammer was used to gradually split the specimens along the predefined paths. To minimize secondary damage such as spalling or unintended cracking, the cutting was performed slowly to reduce mechanical stresses. Additionally, care was taken

Table 5The details of the recorded and measured displacements.

Test No.	$d_{\mathrm{p,i}}\left(\mathrm{mm}\right)$	$d_{\text{B\&W}}$ (mm)	$d'_{p,f}$ (mm)	$D_{p,m}$ (mm)	Ave. $D_{p,m}$ (mm)	δ_{d} (%)
1	34.60	≈ 7	27.60	28.09	31.45	1.70
2	36.07	≈ 6	30.07	34.91		13.90
3	38.08	≈ 7	31.08	31.34		0.80
4	46.98	≈ 8	38.98	47.90	48.72	18.60
5	54.98	≈ 6	48.98	55.84		12.30
6	43.24	≈ 6	37.24	42.42		12.20
7	43.74	≈ 7	36.74	34.81	35.30	5.55
8	41.86	≈ 8	33.86	34.76		5.59
9	44.17	≈ 10	34.17	36.34		5.97

Note: $d_{\text{B\&W}} = l_1 - l_2$; $d^{'}_{\text{p,f}} = (d_{\text{p,i}} - d_{\text{B\&W}})$; and $\delta_{\text{d}} = 100 \times (D_{\text{p,m}} - d^{'}_{\text{p,f}})/D_{\text{p,m}}$.

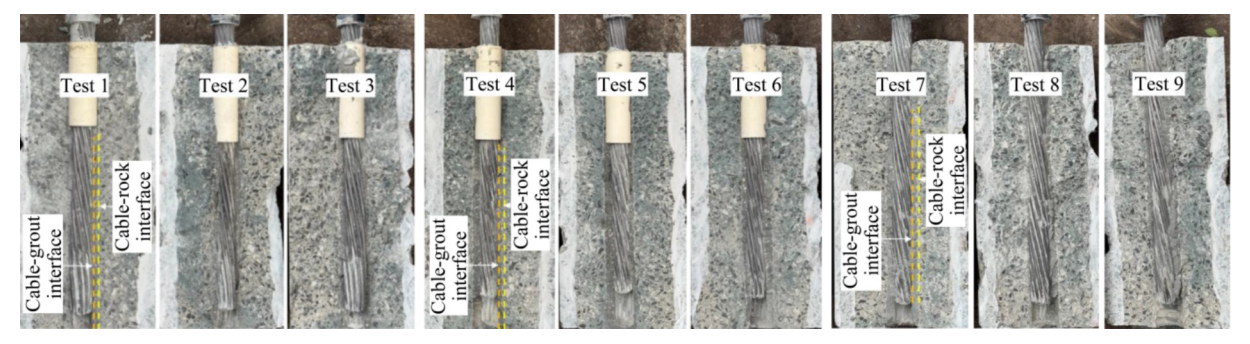


Fig. 21. The post-test observations of the cut-open test samples.

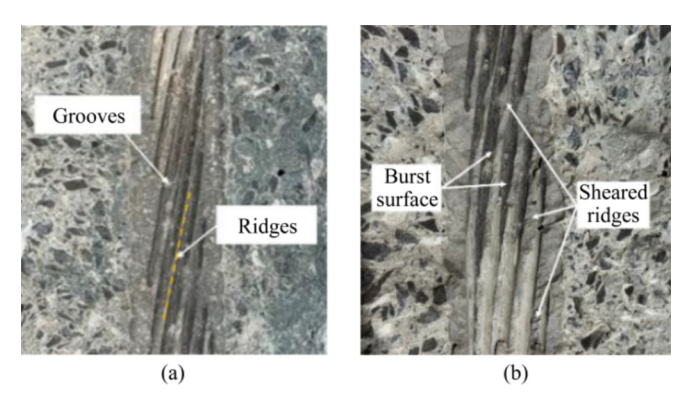


Fig. 22. A view of the grooves and ridges caused by the spiral structure of cable bolt.

to apply controlled force during wedge insertion to avoid introducing secondary cracks or spalling. This method preserved the integrity of the internal features, allowing for accurate visual assessment.

The post-test investigations revealed that the failure mechanism was the debonding of the cable from the grout column, as shown in Fig. 21. In this mode of failure, the shear load, distributed along the cable-grout interface, exceeds the bond strength between the cable and the grout medium.

In addition, as shown in Fig. 22a, due to the spiral structure of the cable wires, the surface of the encapsulation material develops ridges and grooves. The ridges are sharp edges formed by the gaps between wires, while the grooves are the traces of the wire surfaces. Once debonding occurs, the cable bolt begins to move relative to the encapsulation material. This movement can proceed either through the shear failure of the ridges or by sliding along the grooves, which causes the cable to twist around its axial axis. In an impact pull-out test, since the load is applied in a fraction

of time, overcoming the dynamic frictional resistance along the grooves is more feasible than inducing shear failure in the ridges, making untwisting (rotation) and axial movement the dominant mode of displacement.

In this study, the post-test investigations showed that the cable bolts moved in a combination of both frictional sliding along grooves and shear failure of ridges (Fig. 22b). This behavior is supported by the grout surfaces shown in Fig. 23, where the burnt surface of the grooves and moderately broken ridges indicate that frictional sliding. Thus, despite the implementation of antirotation measures during testing, some degree of cable rotation was observed. In experimental studies, some degree of cable rotation may still occur, even when anti-rotation setups are used. This is primarily due to internal strand movement and grout-cable interaction. Since this behavior may lead to a slight underestimation of pull-out performance, particularly in terms of peak load and energy absorption, geotechnical engineers are advised to consider its potential influence when interpreting the findings.

4.3.4. Cable bolt elongation

As mentioned earlier, the obtained plastic displacements might be the result of both cable bolt elongation and displacement. In order to investigate the possibility of the elongation of the cable's wires, the pulled-out and the pulled-in lengths of the cable bolts were manually measured during the post-test inspections, as presented in Table 6. Here, as shown in Fig. 24, the pulled-out length is equal to $D_{p,m}$. For example, in Test 2, the measurements indicated that the cable bolt was pulled out by approximately 35 mm, while it was pulled in by around 31 mm. It was found that, for 300 mm of encapsulation length, the average elongation of the bulbed cable bolts (2.74 mm) is around 2.5 times more than that of the nonbulbed cable bolts (1.11 mm). In addition, the bulbed cable bolts with 450 mm of LE experience lower elongation (1.59 mm) compared to cables with 300 mm of LE. The findings demonstrate that the bulb resists being pulled out. So, it can be inferred that the bulb on the cable bolt functioned as a mechanical anchor, resulting in

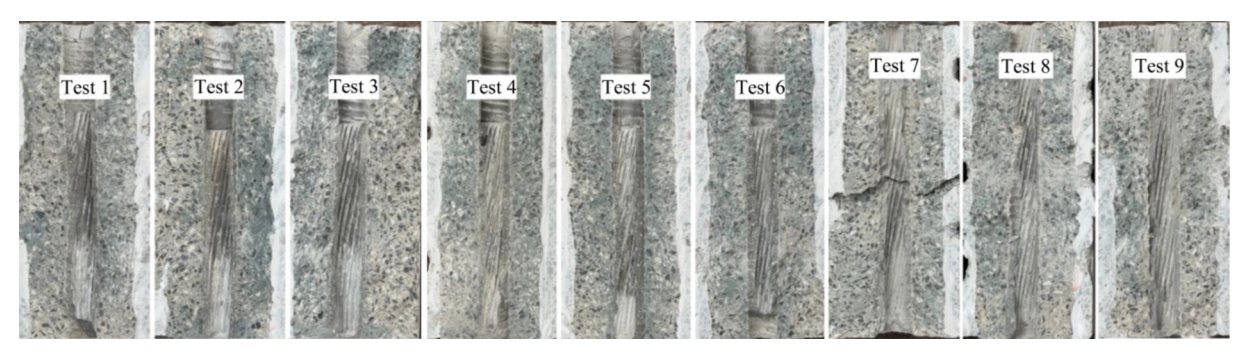


Fig. 23. The post-test conditions of the grout surfaces. Note: the crack appeared in the sample of Test 7 was formed when the sample was cutting open.

Table 6The details of the elongation of the cable bolts during the impact tests.

Test No.	Type	Pulled out length (mm)	Pulled in length (mm)	Elongation (mm)	Ave. elongation (mm)
1	Bulbed	28.09	26.10	1.99	2.76
2	Bulbed	34.91	31.18	3.73	
3	Bulbed	31.34	28.78	2.56	
4	Non-bulbed	47.90	47.52	0.38	1.11
5	Non-bulbed	55.84	53.24	2.60	
6	Non-bulbed	42.42	42.07	0.35	
7	Bulbed	34.81	34.53	0.28	1.59
8	Bulbed	34.76	32.31	2.45	
9	Bulbed	36.34	34.31	2.03	



Fig. 24. A view of measuring the pulled out and pulled in lengths after the impact

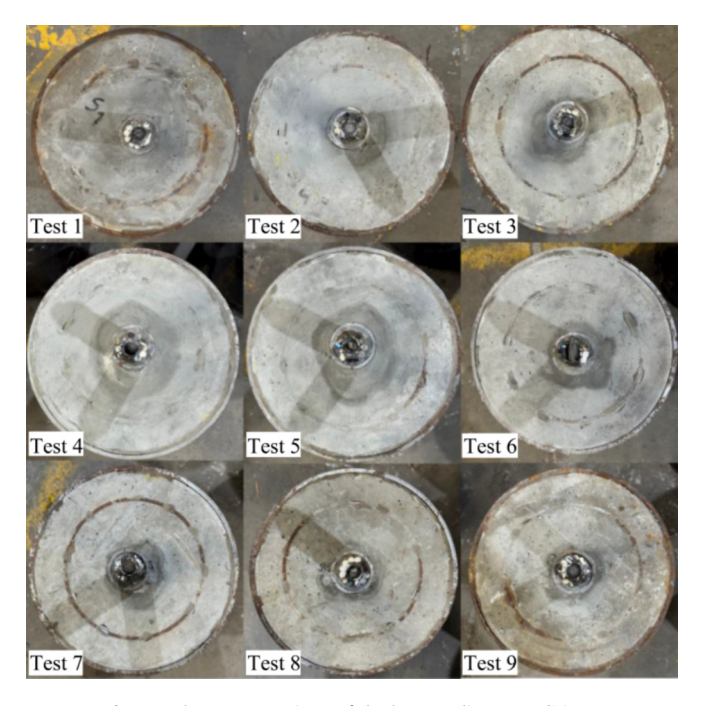


Fig. 25. The post-test views of the host mediums conditions.

the stretching of the cable along the distance between the bulb and the B&W during the impact testing.

4.3.5. Host medium competency

As previously discussed, the structural integrity of the host medium during testing significantly influences the reliability of the results. Once cracking occurs in the concrete specimens, their resistance to pullout forces is considerably reduced. Therefore, it is essential to maintain the rigidity and prevent cracking of the samples throughout the testing process. To achieve this, the concrete specimens in this study were confined both internally and externally using steel pipes. Post-test inspections, as illustrated

in Fig. 25, revealed no visible cracking in any of the samples, including those tested with bulbed cable bolts, which typically induce higher lateral pressures. These observations confirm the effectiveness of the confinement system employed.

4.3.6. Pull-out energy dissipation

The absorbed kinetic energy by the cable bolt, which is consumed for pulling the cable bolt out of the host medium, may be estimated by integrating the area under the pull-out load-displacement curves as given by Eq. (4). *PE* can be referred to as the pull-out energy dissipated through the plastic deformation.

$$PE = \int_0^{d_{\rm p,i}} P \mathrm{d}d \tag{4}$$

where P refers to the pull-out load monitored by the hollow axial load cell at displacement d. The obtained pull-out energies are introduced in Table 7. The test results show that non-bulbed cable bolts absorbed more energy (11.26 kJ) than bulbed cable bolts (8.75 kJ), even when the LE was greater (9.62 kJ). Still, it seems that increasing LE improved the energy absorption capacity of the bulbed cable bolt. Additionally, the energy dissipated by the various test system's parts (E_{sys}) was also estimated. The results showed that energy loss during testing was higher for the bulbed cable bolts (5.19 and 4.32 kJ) compared to the non-bulbed bolts (2.69 kJ). The higher energy absorption capacity observed in non-bulbed cable bolts can be attributed to their greater axial deformability and more distributed bond mobilization. Unlike bulbed cables, which rely on mechanical interlock at discrete bulbed sections, non-bulbed cables mobilise resistance primarily through frictional interaction along the cable-grout interface. This allows for a more gradual and extended slip process, resulting in greater displacement and energy dissipation before failure. Additionally, the absence of bulbed sections reduces localised stress concentrations and grout crushing. promoting a more uniform stress distribution and ductile response under impact loading. These factors collectively contribute to the higher total energy absorption observed in non-bulbed cable bolts, despite their lower peak load resistance.

The findings of this study contradict those reported by Anzanpour et al. [26], despite both studies applying similar input impact energies. This discrepancy is likely due to a combination of factors. In Anzanpour et al. absorbed energy was calculated using a load cell mounted on the impactor, which may not accurately reflect the actual load transferred to the cable bolt due to system losses and dynamic effects. In contrast, the present study employed a load cell mounted directly on the cable bolt, providing a more representative measure of the pull-out load and energy absorption. Besides, beyond instrumentation differences, several material and boundary condition variables must be considered. Anzanpour et al. used 28-mm diameter, 63-t SUMO cable bolts, whereas this study used a 70-t variant with a larger diameter. Differences in tensile strength and wire configuration may influence deformation and energy dissipation behavior.

Table 7The summary of the energy dissipation in the impact tests.

Test No. Bolt type	Bolt type	Bolt type $E_{im,k}$ (kJ)	PE (kJ)		Total energy loss, E_{sys} (kJ)		UPE (kJ/mm)	
			Value	Ave.	Value	Ave.	Value	Ave.
1	Bulbed	13.94	9.84	8.75	4.10	5.19	0.28	0.24
2	Bulbed	13.94	8.64		5.30		0.24	
3	Bulbed	13.94	7.77		6.17		0.20	
4	Non-bulbed	13.94	11.15	11.26	2.79	2.69	0.24	0.23
5	Non-bulbed	13.94	12.36		1.58		0.23	
6	Non-bulbed	13.94	10.26		3.69		0.24	
7	Bulbed	13.94	10.04	9.62	3.90	4.32	0.23	0.22
8	Bulbed	13.94	9.73		4.22		0.23	
9	Bulbed	13.94	9.10		4.85		0.21	

Note: $E_{\text{sys}} = E_{\text{im,k}} - PE$; and $UPE = PE/d_{\text{p,i}}$.

Additionally, the previous study used a grout with a w/c ratio of 0.4, while the present study used a w/c ratio of 0.35, which typically results in higher grout strength and improved bond performance. However, the exact grout type used in the previous study was not reported, limiting direct comparison. Furthermore, although both studies used concrete of the same strength, Anzanpour et al. employed 150-mm diameter steel tubes for internal confinement of the host medium, whereas this study used 200-mm tubes of equal thickness. This difference may influence the concrete's stiffness and energy dissipation characteristics.

These combined differences in measurement technique, cable bolt properties, grout strength, and boundary conditions likely contributed to the observed discrepancy in energy absorption values. Acknowledging these factors is essential for interpreting comparative results and highlights the need for standardised testing protocols in future dynamic cable bolt research.

4.3.7. Rock support system in burst-prone grounds

Table 7 presents the calculated unit pull-out energy (UPE), defined as the ratio of absorbed energy to the corresponding displacement during impact testing. This metric reflects the energy required to pull the cable bolt by 1 mm and serves as an indicator of the system's resistance to dynamic loading. The highest UPE value was recorded for bulbed cable bolts with 300 mm encapsulation length, reaching 0.243 kJ/mm, which suggests initial anchorage and resistance to pull-out forces.

However, in burst-prone ground conditions, the ability of a support system to absorb energy and accommodate deformation is more critical than peak resistance alone [13]. Rockburst events typically involve rapid energy release and large displacements, and support systems must dissipate this energy effectively to prevent structural failure. In this context, non-bulbed cable bolts, despite having lower UPE, demonstrated greater total energy absorption and displacement capacity, making them more suitable for dynamic environments where post-failure deformation control is essential.

To further contextualize these findings, rockburst events in deep mining operations can release energy ranging from 10 to 50 kJ/m², with ejection velocities between 3 and 10 m/s, depending on geological conditions and mining depth [11,12]. The tested impact velocity of 6.86 m/s and energy level of 14.52 kJ in this study correspond to moderate to severe rockburst scenarios, commonly observed in deep coal mines and hard rock environments. In such conditions, geological strata like highly stressed quartzite, dolomite, or coal seams with stiff roof layers demand support systems capable of both high energy dissipation and large deformation accommodation. The greater displacement and energy absorption capacity of non-bulbed cable bolts observed in this study suggest their suitability for these high-energy, high-deformation environments. In contrast, bulbed cable bolts, which

exhibit higher initial peak loads, may be more appropriate in brittle rock formations with low deformation tolerance, where immediate anchorage strength is critical. These insights can guide engineers in selecting cable bolt types based on expected rockburst intensity and geological context, contributing to safer and more resilient ground support systems.

Additionally, it is noteworthy that no single type of cable bolt or rock bolt is capable of independently resisting the impact loading associated with rockburst [13]. In fact, designing a system capable of withstanding all possible seismic events is practically impossible. Effective mitigation requires an integrated support system combining components that are able to demonstrate high energy dissipation capacity, deformability, and mechanical connection. In this regard, Li [24] highlights that various support strategies have been developed globally to address rockburst hazards, with empirical evidence suggesting that fully yieldable support systems, including cable bolts, energy-absorbing rock bolts, and surface retention elements such as wire mesh and shotcrete, offer better performance.

It becomes evident that, rather than relying solely on a fully robust support system, a resilient support system may offer better performance in mitigating the effects of rockbursts. In this regard, the performance of support systems can be compared schematically based on their resiliency level by using Fig. 26. As can be seen, initially, all three systems experience a gradual decline in performance due to factors such as aging, static loading, and environmental degradation. At time T1, a seismic event (e.g., rockburst) takes place. System "A" (Fig. 26a), which has been designed with high resistance/robustness, initially absorbs the impact energy. Nevertheless, once the stress imposed by the seismic event exceeds the system's capacity, it experiences catastrophic failure, resulting in a sudden and complete loss of functionality, leading to severe consequences such as ground collapse.

In contrast, system "B" (Fig. 26b), demonstrates the capacity to absorb and adapt to the impact without experiencing abrupt failure. Although it may suffer a temporary reduction in performance, it maintains its core value/functionality, so preventing catastrophic outcomes. This adaptability allows the system to continue providing essential support functions during and after the event. However, if the damaged components of the support system are left unrepaired, due to various parameters like management issues, design issues, and lack of budget and facilities, the system becomes vulnerable to failure, even during low magnitude seismics events. Therefore, simply having flexible support systems is not adequate to ensure the ground stability in burst-prone grounds.

Instead, a resilient system (Fig. 26c) not only maintains its core performance by impact energy absorption, but can also be restored through recovery measures, such as repairing or replacing damaged components like wire meshes and bolts. Then, the system performance can be restored to its original or near-original perfor-

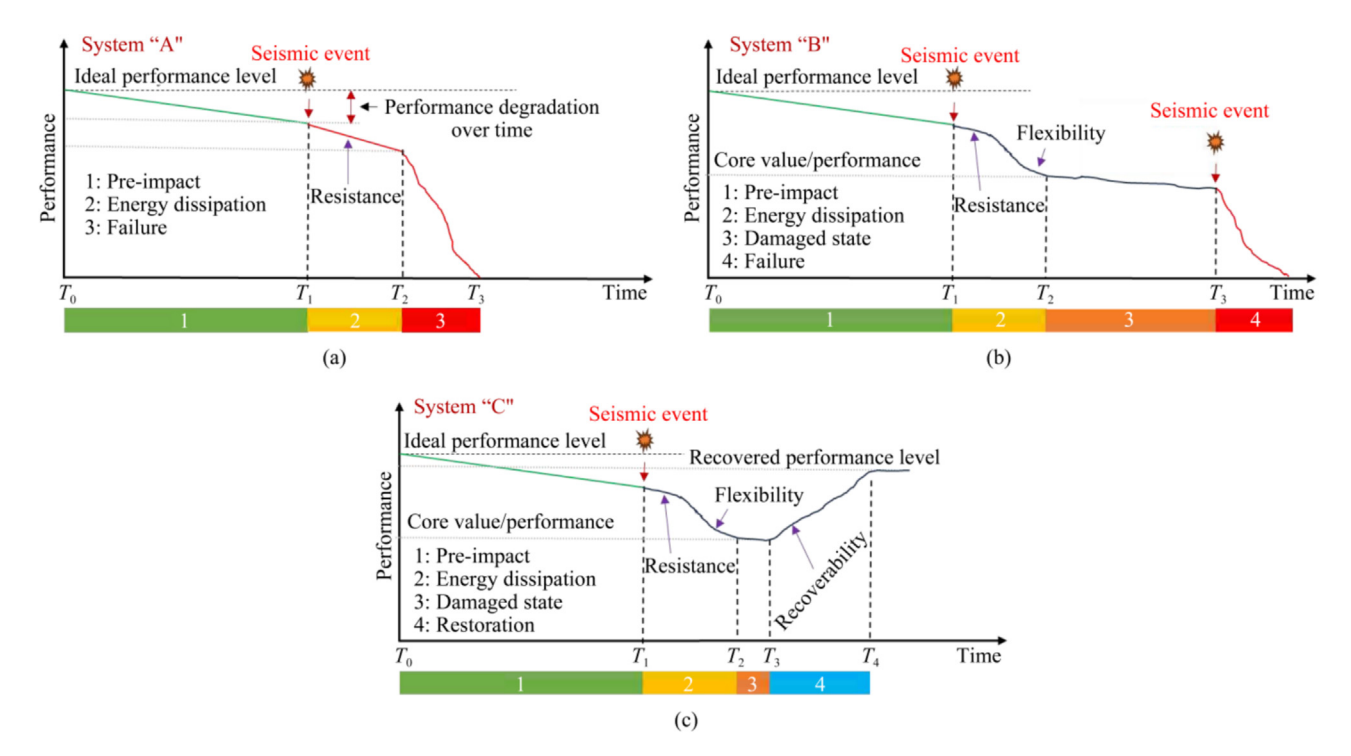


Fig. 26. A schematic comparison between support systems having various levels of resiliency.

mance level. Therefore, the concept of resilience can be employed in the domain of burst-prone grounds to form resilient support systems characterized by their ability to resist, absorb, accommodate, and recover from seismic events in a timely and efficient manner, for the preservation and restoration of essential services [54]. This can serve as a potential research direction for exploring strategies to design resilient support systems.

5. Research limitations

While the conducted study offers valuable insights into the performance of cable bolts under impact loading conditions, several important limitations should be acknowledged as follows:

5.1. Replicating in-situ condition by using RPTM

Although the RPTM offers a controlled and repeatable laboratory setup for evaluating the dynamic performance of cable bolts, its ability to replicate actual underground field conditions is limited. The use of concrete as a host medium, while practical and consistent for laboratory testing, does not fully capture the heterogeneity, jointing, and anisotropic behaviour of natural rock masses. These differences may influence load transfer mechanisms, failure modes, and energy dissipation characteristics. Additionally, the confinement conditions and boundary interactions in the lab differ from those encountered in underground excavations, where stress redistribution is a significant factor. Therefore, while the results provide valuable insights into cable bolt behaviour under impact loading, caution should be applied when generalising these findings to field applications. Future research should include in-situ testing, numerical modelling calibrated with field data, and comparative studies using more representative host media to enhance the transferability of laboratory results to real underground environments.

5.2. Cable rotation

Although cable bolts are generally designed to resist unscrewing under field conditions, some degree of rotation may still occur. especially in deep or seismically active environments. Thus, understanding the influence of cable rotation on performance remains important for realistic assessment. Additionally, in this study, despite the use of an anti-rotation system, cable rotation was still observed during impact testing. Such a movement may lead to an underestimation of the cable bolt's load-bearing capacity. However, although the quantitative impact of cable rotation is difficult to isolate, as it involves complex interactions between axial loading, interface friction, and cable deformation mechanisms, to address this issue, the future comparative studies should be undertaken under both free and restricted rotation scenarios. This will help quantify the influence of cable rotation and allow for more accurate interpretation and comparison of cable bolt performance under impact loading.

5.3. Encapsulation length

It is recognised that a broader parametric analysis, including intermediate encapsulation lengths, would enhance the comprehensiveness of the study. This limitation needs to be addressed in future work by expanding the testing matrix to include a wider range of parameters, thereby enabling more robust performance relationships and practical design recommendations for dynamic ground support systems. Furthermore, it is acknowledged that the encapsulation length may influence the failure interface. Although debonding at the cable-grout interface was consistently observed in this study, future research should investigate a broader range of encapsulation lengths to better understand their effect on failure mechanisms.

International Journal of Mining Science and Technology xxx (xxxx) xxx

5.4. Input impact energy

Another limitation of this study is the use of a fixed input impact energy of 14.52 kJ, corresponding to an impact velocity of 6.86 m/s. Although this configuration was designed to simulate moderate to severe rockburst conditions, it does not capture the full spectrum of dynamic loading scenarios encountered in underground environments. The use of a single energy level restricts the ability to assess cable bolt performance under varying rockburst intensities. To enhance the applicability of the findings, future studies should incorporate variable input energies and velocities to simulate a broader range of field conditions and better understand the energy absorption behaviour of cable bolts across different dynamic loading regimes.

5.5. Displacement deviations

Discrepancies were found between instrument-based and manual displacement measurements, potentially introducing bias. Instrument readings may be affected by calibration offsets due to mounting misalignment or transient vibrations during impact. Manual measurements, taken post-test through visual inspection, are prone to human error and subjective interpretation. To improve accuracy in future studies, high-speed video tracking is recommended.

6. Conclusions

This experimental study contributes to the understanding of high-strength cable bolt performance when subjected to impact loading, a critical area for enhancing safety and productivity in underground mining and tunnelling operations. The key findings are summarized as follows:

- (1) First peak load: Bulbed cable bolts demonstrated a higher average *FPL* of approximately 328 kN, compared to 218 kN for non-bulbed cables at 300 mm encapsulation length. This is attributed to the mechanical anchoring effect of the bulbed cable bolts, which provides higher initial resistance to pull-out.
- (2) Displacement capacity: The tested non-bulbed cable bolts showed greater plastic displacement, averaging 48.40 mm, versus 36.25 mm for the bulbed cable bolts.
- (3) Energy absorption: The non-bulbed cable bolts absorbed more total pull-out energy, with an average of 11.26 kJ, compared to 8.75 kJ for the bulbed cable bolts.
- (4) Impact duration: The non-bulbed cable bolts sustained the impact load for a longer duration (28.50 ms) compared to the bulbed cable bolts (19.80 ms), indicating a more prolonged and effective energy absorption process.
- (5) Effect of encapsulation length: Increasing encapsulation length for the bulbed cable bolts reduced initial peak load from 328 to 248 kN, but improved axial displacement from 36.25 to 43.26 mm and increased impact duration from 19.80 to 22.37 ms. However, more experiments are needed to draw a conclusive conclusion on the influence of the encapsulation length in the context of impact loading.
- (6) Failure mechanism: The primary failure mechanism observed for both cable types was debonding at the cable-grout interface, often involving a combination of frictional sliding and shear failure, with some unavoidable cable rotation despite antirotation measures.

Although the bulbed cables are more efficient in absorbing energy per unit of displacement, the non-bulbed cable's capacity for larger total displacement and energy absorption makes them potentially more effective in dynamically active grounds where accommodating considerable rock mass deformation is essential

for rockburst control. The study also highlighted the importance of a resilient support system in rockburst-prone grounds, emphasising that no single cable bolt type can independently resist impact loading. Instead, an integrated system combining high energy dissipation, deformability, mechanical connection, and recoverability is essential.

While this research offers useful contributions, future studies should address the limitations to further refine understanding and improve the design of integrated support systems for rockburst mitigation. Thus, future research should aim to expand the experimental scope with larger sample sizes and diverse cable bolt types, enhance measurement accuracy through advanced instrumentation, and improve the anti-rotation system. This continued research is vital for developing the engineering understanding which is necessary to improve the resilience and safety of underground infrastructure against seismic events.

CRediT authorship contribution statement

Adel Mottahedi: Writing – review & editing, Writing – original draft, Visualization, Methodology, Investigation, Formal analysis, Conceptualization. **Naj Aziz:** Writing – review & editing, Validation, Supervision, Methodology, Formal analysis, Conceptualization. **Alex Remennikov:** Writing – review & editing, Validation, Supervision, Conceptualization. **Ali Mirzaghorbanali:** Writing – review & editing, Validation, Supervision, Methodology.

Declaration of competing interest

The authors declare that they have no known competing financial interests or personal relationships that could have appeared to influence the work reported in this paper.

Acknowledgments

The authors would like to express their appreciation to Jennmar Australia Pty Ltd for supplying the required materials and the university personnel who assisted in completing the tests conducted at the University of Wollongong, especially Mr. Travis Marshall and Mr. Ritchie McLean.

References

- [1] Mottahedi A, Aziz N, Remennikov A, Mirzaghorbanali A, Marston K. A critical review on development of laboratory testing technologies of tendons applied to stabilize underground structures. Rock Mech Rock Eng 2025;58(7):7531–67.
- [2] Hutchinson DJ, Diederichs MS. Cablebolting in Underground Mines. Richmond: BiTech Publishers; 1996.
- [3] Jodeiri Shokri B, Mirzaghorbanali A, Nourizadeh H, McDougall K, Karunasena W, Aziz N, Entezam S, Entezam A. Axial load transfer mechanism in fully grouted rock bolting system: A systematic review. Appl Sci 2024;14(12):5232.
- [4] Fuller P. Pre-reinforcement of cut and fill stopes. In: Proceedings of the conference on application of rock mechanics to cut-and-fill mining. Lulea, Sweden; 1981.p.155–79.
- [5] Galvin JM. Support and reinforcement systems. In: Ground engineering: Principles and practices for underground coal mining. Cham: Springer International Publishing; 2016. p. 211–69.
- [6] Thompson AG, Villaescusa E. Case studies of rock reinforcement components and systems testing. Rock Mech Rock Eng 2014;47(5):1589–602.
- [7] Windsor CR. Rock reinforcement systems. Int J Rock Mech Min Sci 1997;34 (6):919–51.
- [8] Hadjigeorgiou J, Potvin Y. A critical assessment of dynamic rock reinforcement and support testing facilities. Rock Mech Rock Eng 2011;44(5):565–78.
- [9] Li CC, Mikula P, Hadjigeorgiou J, Simser B, He MC, Canbulat I, Joughin W. ISRM suggested method for determining the properties of rock bolt assemblies by mass freefall impact testing in the laboratory. Rock Mech Rock Eng 2025;58 (1):165–79.
- [10] Tannant DD, Brummer RK, Yi X. Rockbolt behaviour under dynamic loading: Field tests and modelling. Int J Rock Mech Min Sci Geomech Abstr 1995;32 (6):537–50.
- [11] Player J, Thompson A, Villaescusa E. Dynamic testing of reinforcement systems. In: Proceedings of the 6th international symposium on ground

- support in mining and civil engineering construction. Kalgoorlie: Western Australia School of Mines. 2008, p. 597–622.
- [12] St-Pierre L, Hassani FP, Radziszewski PH, Ouellet J. Development of a dynamic model for a cone bolt. Int J Rock Mech Min Sci 2009;46(1):107–14.
- [13] Cai M. Principles of rock support in burst-prone ground. Tunn Undergr Space Technol 2013;36:46–56.
- [14] Stacey TR, Rojas E. A potential method of containing rockburst damage and enhancing safety using a sacrificial layer. J S Afr N Inst Min Metall 2013:113:565–73.
- [15] Mottahedi A, Aziz N, Remennikov A, Mirzaghorbanali A, Marston K. Impact loading of tendon reinforcement systems used for ground control: A critical literature review. Arch Min Sci 2024:711–43.
- [16] Li CC, Hadjigeorgiou J, Mikula P, Knox G, Darlington B, Royer R, Pytlik A, Hosp M. Performance of identical rockbolts tested on four dynamic testing rigs employing the direct impact method. J Rock Mech Geotech Eng 2021;13 (4):745-54.
- [17] Yan C. Bond between reinforcing bars and concrete under impact loading. Doctoral dissertation. Vancouver: University of British Columbia Library; 1992. p. 64.
- [18] Ansell A. Laboratory testing of a new type of energy absorbing rock bolt. Tunn Undergr Space Technol 2005;20(4):291–300.
- [19] Chunlin LC. A new energy-absorbing bolt for rock support in high stress rock masses. Int J Rock Mech Min Sci 2010;47(3):396–404.
- [20] Li CC, Doucet C. Performance of D-bolts under dynamic loading. Rock Mech Rock Eng 2012;45(2):193–204.
- [21] Knox G, Berghorst A. Dynamic testing: Determining the residual dynamic capacity of an axially strained tendon. In: Proceedings of the 9th international symposium on ground support in mining and underground construction. Perth: Australian Centre for Geomechanics; 2019. p.231–42.
- [22] Crompton B, Knox G. Dynamic testing: Determining the relationship between rockbolt diameter and the residual dynamic capacity of an axially strained tendon. In: Proceedings of the 5th international conference on block and sublevel caving. Perth: Australian Centre for Geomechanics; 2022. p.141–51.
- [23] Darlington B, Vallati O, Young P. A comparison between laboratory and in situ dynamic testing on the MDX bolt. In: Proceedings of the 10th international conference on ground support in mining. Perth: Australian Centre for Geomechanics; 2023. p.361–70.
- [24] Li CC. Principles and methods of rock support for rockburst control. J Rock Mech Geotech Eng 2021;13(1):46–59.
- [25] Anzanpour S, Aziz N, Memcik J, Mirzaghorbanali A, Wallace J, Marshall T, Khaleghparast S. Introduction to new methods of static and dynamic pull testing of rock bolts and cable bolts. In: Proceedings of the 2021 resource operators conference. Wollongong: University of Wollongong; 2021. p.210– 17.
- [26] Anzanpour S, Aziz N, Nemcik J, Remennikov A, Mirzaghorbanali A, Wallace J. Static and dynamic tendon pull-out test research at the University of Wollongong. In: Proceedings of the 2022 resource operators conference. Wollongong: University of Wollongong; 2022. p.182–89.
- [27] Ortlepp W, Stacey T. Testing of tunnel support: Dynamic load testing of rockbolt elements to provide data for safer support design. Safety in Mines Research Advisory Committee 1998:3.
- [28] Villaescusa E, Thompson A, Player J. Dynamic testing of rock reinforcement systems. In: Proceedings of the Australian mining technology conference. Fremantle: Australasian Institute of Mining and Metallurgy, p. 79–95.
- [29] Pytlik A, Szot M. Comparative testing of cable bolt and wire rope lacing resistance to static and dynamic loads. Arch Min Sci 2023;68(4):707–24.
- [30] JENNMAR coal catalogue. Jennmar Australia Pty Ltd; 2025. p.22–4.
- [31] Thenevin I, Blanco-Martín L, Hadj-Hassen F, Schleifer J, Lubosik Z, Wrana A. Laboratory pull-out tests on fully grouted rock bolts and cable bolts: Results and lessons learned. J Rock Mech Geotech Eng 2017;9(5):843–55.
- [32] Bawden WF, Hyett AJ, Lausch P. An experimental procedure for the in situ testing of cable bolts. Int J Rock Mech Min Sci Geomech Abstr 1992;29 (5):525–33.

- [33] Clifford B, Kent L, Altounyan P, Bigby D. Systems used in coal mining development in long tendon reinforcement. In: Proceedings of the 20th international conference on ground control in mining. West Virginia: International Conference on Ground Control in Mining. p. 235–41.
- [34] Chen JH, Hagan PC, Saydam S. A new laboratory short encapsulation pull test for investigating load transfer behavior of fully grouted cable bolts. Geotech Test J 2018;41(3):435–47.
- [35] Anzanpour S. The load transfer mechanism of ground tendons subjected to static and dynamic loading conditions. Doctoral dissertation. Wollongong: University of Wollongong; 2022. p162.
- [36] Chen JH, Hagan PC, Saydam S. Sample diameter effect on bonding capacity of fully grouted cable bolts. Tunn Undergr Space Technol 2017;68:238–43.
- [37] Kaewunruen S. Experimental and numerical studies for evaluating dynamic behaviour of pre-stressed concrete sleepers subject to severe impact loading. J Proc R Soc N S W 2008;141(3-4):52-3.
- [38] Khaleghparast S, Aziz N, Remennikov A, Anzanpour S. An experimental study on shear behaviour of fully grouted rock bolt under static and dynamic loading conditions. Tunn Undergr Space Technol 2023;132:104915.
- [39] Chen Y, Li CC. Influences of loading condition and rock strength to the performance of rock bolts. Geotech Test J 2015;38(2):208–18.
- [40] Han JY, Liu D, Guan YP, Chen Y, Li TL, Jia DF, Yan FS, Jia PJ, Zhao Y. Study on shear behavior and damage constitutive model of tendon-grout interface. Constr Build Mater 2022;320:126223.
- [41] Hyett AJ, Bawden WF, Reichert RD. The effect of rock mass confinement on the bond strength of fully grouted cable bolts. Int J Rock Mech Min Sci Geomech Abstr 1992;29(5):503–24.
- [42] Klar A, Nissim O, Elkayam I. A hardening load transfer function for rock bolts and its calibration using distributed fiber optic sensing. J Rock Mech Geotech Eng 2023;15(11):2816–30.
- [43] Aziz N, Yang G, Khaleghparast S, Marshall T. Development of double shear testing of tendons. In: Proceedings of the 2019 Coal Operators' Conference. Wollongong: University of Wollongong; 2019. p.150–161.
- [44] Blanco Martín L, Tijani M, Hadj-Hassen F, Noiret A. Assessment of the bolt-grout interface behaviour of fully grouted rockbolts from laboratory experiments under axial loads. Int | Rock Mech Min Sci 2013;63:50–61.
- [45] AS_1012.17. Australian Standards: Methods of testing concrete determination of the static chord modulus of elasticity and Poisson's ratio of concrete specimens; 1997. p.3.
- [46] AS_1012.14. Australian Standard: Method for testing concrete, and method for securing and testing cores from hardened concrete for compressive strength and mass per unit volume; 2018. p.4.
- [47] Hagan P, Li D, Masoumi H, Saydam S. Performance of cable bolts under axial loading subjected to varying geotechnical conditions. UNSW Sydney 2017:9.
- [48] ACI Committee 308. Standard practice for curing concrete (ACI308-92). American Concrete Institute (ACI); 1980. p.4.
- [49] Zhang YY, Pan RY, Xiao F. Numerical research on impact performance of bridge columns with aluminum foam protection devices. Int J Distrib Sens Netw 2020;16(11). 155014772097453.
- [50] Knox G, Berghorst A. Increased agility for the research and development of dynamic roof support products. In: Rock Dynamics and Applications 3. Boca Raton: CRC Press; 2018. p.373–78.
- [51] Sharma HK, Sharma RK, Saxena RS, Prasad R. A review of nanoindentation and related cathodoluminescence studies on semiconductor materials. J Mater Sci Mater Electron 2022;33(27):21223–45.
- [52] Rajaie H. Experimental and numerical investigations of cable bolt support systems. Doctoral dissertation. Montreal: McGill University; 1990. p. 126.
- [53] Ren FF, Yang ZJ, Chen JF, Chen WW. An analytical analysis of the full-range behaviour of grouted rockbolts based on a tri-linear bond-slip model. Constr Build Mater 2010;24(3):361–70.
- [54] Mottahedi A, Sereshki F, Ataei M, Qarahasanlou AN, Barabadi A. Resilience estimation of critical infrastructure systems: Application of expert judgment. Reliab Eng Syst Saf 2021;215:107849.